IASI L2 PPF v6.4 validation report

Doc.No. : EUM/RSP/REP/18/974859
Issue : v1 e-signed
Date : 26 February 2018
WBS/DBS :

EUMETSAT
Eumetsat-Allee 1, D-64295 Darmstadt, Germany
Tel: +49 6151 807-7
Fax: +49 6151 807 555
http://www.eumetsat.int

This page intentionally left blank

Document Change Record

Version	***Date of Version*** *as on profile*	***Document Change Request (DCR) Number*** *if applicable*	***Description of changes***
V1	26/02/2018		Initial version

Table of Contents

1 INTRODUCTION....7
1.1 Purpose....7
1.2 Background and scope....7
1.3 Applicable Documents....7
1.4 Reference Documents....8
1.5 Acronyms....9

2 PROCESSOR CHANGES AND VALIDATION DATA DESCRIPTION....11
2.1 IASI L2 processor overview....11
2.2 Algorithms and products updates....12
2.3 Processor versioning....12
2.4 Assessment of temperature and humidity with radiosondes....13
2.5 Stratification of comparisons to ECMWF analyses....13

3 PWLR^3: FIRST RETRIEVAL OF TEMPERATURE AND HUMIDITY PROFILES....15
3.1 Comparison of reprocessed IR-only PWLR^3 retrievals to radiosondes....16
3.2 Comparison of reprocessed MW+IR PWLR^3 retrievals to radiosondes....22
3.3 Assessment of the quality indicator for temperature with radiosondes....26

4 OEM RETRIEVALS WITH UPDATED RTTOV COEFFICIENTS....28
4.1 v6.3 and v6.4 temperature profiles vs radiosondes....28
4.2 v6.3 and v6.4 humidity profiles vs radiosondes....29
4.3 v6.3 and v6.4 temperature profiles vs ECMWF analysis....30
4.4 v6.3 and v6.4 humidity profiles vs ECMWF analysis....34

5 ASSESSMENT OF THE SEA SURFACE TEMPERATURE....37
5.1 IASI v6.3 and v6.4 SST vs OSTIA....37
5.2 IASI v6.3 and v6.4 SST vs ECMWF analysis....41
5.3 Comparisons against buoy SST with the OSI SAF matchup dataset....46

6 ASSESSMENT IN RADIANCE SPACE OF THE PARAMETERS RETRIEVED WITH THE FIRST RETRIEVAL (PWLR^3)....47
6.1 Focus on land surface emissivity....47
6.2 Zoom in the ozone region....49
6.3 Residuals from v6.3 (GS1), v6.4 (GS2) and NWP forecasts in IASI bands 1 and 2....50
6.3.1 Maritime scenes....50
6.3.2 Continental scenes....52

7 VERIFICATION OF REGIONAL AND GLOBAL PROCESSING....54

8 SUMMARY AND RECOMMENDATIONS....58

Table of Figures

Figure 1: IASI L2 processing sequence....11
Figure 2: Geographic classes used in the IASI L2 validation....14
Figure 3: Standard deviation of the temperature difference between sonde measurements and IR-only PWLR^3 retrievals from IASI-A (top) and IASI-B (bottom) in the 600-800 hPa layer between January and October 2017....16
Figure 4: Match-up counts at each sonde site with the IR-only PWLR^3 retrievals from IASI-A (top) and IASI-B (bottom) between January and October 2017....17
Figure 5: Differences (solid: bias, dash: standard deviation) between radiosonde measurements and IR-only PWLR^3 retrievals from Metop-A in temperature (top) and humidity (bottom), January to October 2017....18
Figure 6: Same as previous, for Metop-B....19

Figure 7: Time series of temperature and humidity differences between IR-only PWLR^3 retrievals from Metop-A and radiosondes at 500 hPa, from January to October 2017. 20
Figure 8: Same as previous, for Metop-B. 21
Figure 9: Standard deviation of the temperature difference between sonde measurements and MW+IR PWLR^3 retrievals from IASI-A (top) and IASI-B (bottom) in the 600-800 hPa layer between January and October 2017. 22
Figure 10: Match-up counts of sonde collocations with the MW+IR PWLR^3 retrievals from IASI-A (top) and IASI-B (bottom) between January and October 2017. 23
Figure 11: Differences (solid: bias, dash: standard deviation) between radiosonde measurements and MW+IR PWLR^3 retrievals from Metop-A in temperature (top) and humidity (bottom), January to October 2017. 24
Figure 12: Same as previous, from Metop-B 25
Figure 13: Differences between IASI PWLR^3 temperature (left: IR-only, right: MW+IR) and radiosondes, stratified with the quality indicator for temperature, from January to October 2017. 26
Figure 14: Relative sample size of the five quality classes for temperature, with the IR-only (left) and MW+IR (right) retrievals. 26
Figure 15: Maps of the standard deviation (IASI temperature vs sondes) in the layer 600-800 hPa with the IR-only (left) and MW+IR (right) modes for the five quality classes defined in Figure 3 27
Figure 16: Standard deviation of the temperature difference between sonde measurements and OEM retrievals from IASI-A in the 600-800 hPa layer between 23/12/2017 and 13/02/2018. 29
Figure 17: Metop-A (left) and Metop-B (right) temperature retrievals compared to radiosondes between 23 December 2017 and 13 February 2018 with the processor v6.3 (cyan: PWLR^3, blue: OEM) and v6.4 (orange: PWLR^3, red:OEM) 29
Figure 18: Metop-A (left) and Metop-B (right) temperature retrievals compared to radiosondes between 23 December 2017 and 13 February 2018 with the processor v6.3 (cyan: PWLR^3, blue: OEM) and v6.4 (orange: PWLR^3, red:OEM) 30
Figure 19: Comparison of temperature profiles from IASI L2 v6.3 (blue:OEM, cyan:PWLR^3) and v6.4 (red: OEM, orange:PWLR^3) to ECMWF analyses in regional classes, from Metop-B between 1 and 13 February 2018. 32
Figure 20: Comparison of temperature profiles from IASI L2 v6.3 (blue:OEM, cyan:PWLR^3) and v6.4 (red: OEM, orange:PWLR^3) to ECMWF analyses in regional classes, from Metop-A between 1 and 13 February 2018. 33
Figure 21: Comparison of humidity profiles from IASI L2 v6.3 (blue:OEM, cyan:PWLR^3) and v6.4 (red: OEM, orange:PWLR^3) to ECMWF analyses in regional classes, from Metop-B between 1 and 13 February 2018. 35
Figure 22: Comparison of humidity profiles from IASI L2 v6.3 (blue:OEM, cyan:PWLR^3) and v6.4 (red: OEM, orange:PWLR^3) to ECMWF analyses in regional classes, from Metop-A between 1 and 13 February 2018. 36
Figure 23: L2P SST monitoring in December 2017, IASI in cyan 38
Figure 24: Anomaly in the IASI SST L2P product vs OSTIA (top left: day, top right: night) due to cloud misclassification (bottom MODIS RGB) 38
Figure 25: IASI vs OSTIA SST monitoring (QL 3 to 5) on 27 January 2018. The outliers in v6.3 (top, red ellipses) are filtered in v6.4 (bottom) as a result of updated quality control. 39
Figure 26: Routine daily monitoring of IASI L2P SST (left: operational v6.3 ; right: v6.4 in validation) vs OSTIA for day (top) and night (bottom) observations, on 05/02/2018. 40
Figure 27: Quality class 5 (best) IASI L2P SST v6.3 (blue) and v6.4 (red) vs ECMWF skin SST analyses between 1 and 13 February 2018. Metop-B (left) and Metop-A (right) at day (top) and night (bottom). 42
Figure 28: Quality class 4 (high) IASI L2P SST v6.3 (blue) and v6.4 (red) vs ECMWF skin SST analyses between 1 and 13 February 2018. Metop-B (left) and Metop-A (right) at day (top) and night (bottom). 43
Figure 29: Quality class 3 (good) IASI L2P SST v6.3 (blue) and v6.4 (red) vs ECMWF skin SST analyses between 1 and 13 February 2018. Metop-B (left) and Metop-A (right) at day (top) and night (bottom). 44
Figure 30: Quality class 2 (low – not for use) IASI L2P SST v6.3 (blue) and v6.4 (red) vs ECMWF skin SST analyses between 1 and 13 February 2018. Metop-B (left) and Metop-A (right) at day (top) and night (bottom). 45
Figure 31: Location of pixels used in Figure 32, 01/11/2017 47

Figure 32: Continental OBS-CALC with different land surface emissivity dataset: PWLR^3 LSE (red) and CAMEL static (black). Metop-B, mid- and low-lat on 01/11/2017....48
Figure 33: Same as Figure 32, in the Polar caps, with |lat|>60°....48
Figure 34: Same as Figure 32 with the addition (in blue) of CALC computed with ECMWF forecasts + static emissivity atlas....49
Figure 35: Maritime OBS-CALC with different ozone datasets: CAMS (purple), ECMWF FCT (blue), ERA-5 (red), PWLR^3 (black). Metop-B, mid- and low-lat on 01/12/2016....50
Figure 36: Maritime OBS-CALC computed with PWLR^3 v6.3 (from GS1, red), PWLR^3 v6.4 (from GS2, black) and with ECMWF forecasts (blue). Metop-B cloud-free pixels from 1 to 3 February 2018 51
Figure 37: Same as Figure 36, with the same SST (from OEM v6.4) for all 3 OBS-CALC....51
Figure 38: Continental OBS-CALC computed in IASI band 1 with PWLR^3 v6.3 (from GS1, red), PWLR^3 v6.4 (from GS2, black) and with ECMWF forecasts (blue). Metop-B cloud-free pixels from 1 to 3 February 2018....52
Figure 39: Same as Figure 38, in IASI band 2 (water-vapour region)....53
Figure 40: High level overview of the IASI L2 functions retained for regional processing in EARS-IASI L2....54
Figure 41: EARS IASI geographical coverage....54
Figure 42: Regional vs global IASI L2 temperature (solid: bias, dash: standard deviation) on 16 February 2018. Overall statistics is in blue and robust statistics (within the ±3σ range) is in red (left: Metop-A, right: Metop-B)....56
Figure 43: Regional vs global IASI L2 humidity (solid: bias, dash: standard deviation) on 16 February 2018. Overall statistics is in blue and robust statistics (within the ±3σ range) is in red (left: Metop-A, right: Metop-B)....56
Figure 44: Histogram of the differences between IASI L2 regional and global surface temperature [land and sea combined] on 16 February 2018 (left: Metop-A, right: Metop-B). In blue: overall statistics, in red: robust statistics within 3σ....57
Figure 45: Maps of outliers between regional and global surface skin temperature, for Metop-A (left) and –B (right) on 16 February 2018....57

Table of Tables

Table 1: Definition of the validation geographic classes....14
Table 2: Summary of the differences IASI L2Pcore SST – ECMWF analyses in each quality classes. Daytime products between 1 and 13 February 2018....46
Table 3: Summary of the differences IASI L2Pcore SST – ECMWF analyses in each quality classes. Night-time products between 1 and 13 February 2018....46

1 INTRODUCTION

1.1 Purpose

The document presents assessment results of the IASI Level 2 (L2) products generated with the IASI L2 Product Processing Facility (PPF) version 6.4 (v6.4). The v6.4 is the fourth incremental upgrade to the IASI L2 processor since the operational release of the version 6 in September 2014.

1.2 Background and scope

This report is addressed to all Users of the IASI L2 products. It informs about the motivation and nature of processing changes and provides detailed information about the IASI L2 sounding products performances in terms of yield/coverage and precision. It illustrates the continuity and improvements as compared to the former revisions.

This validation report is also addressed to the Product Validation Review Board, to complete the qualification process for this new revision and support its release in operations.

Extensive validation studies were carried out for the release of the IASI L2 processor version 6. The uncertainties assessments have been performed by comparisons to *in situ* (e.g. atmospheric radio-sondes, maritime buoys...) and ground-based measurements (e.g. precipitable water-vapour with radio-occultation instruments, Lidars, Microwave atmospheric sounders, land surface radiometers...), as well as comparisons to numerical models or to other satellite data. The results can be found in the IASI L2 v6 validation reports [RD-1, RD-2, RD-3, RD-7] and in external validation papers [RD-4, RD-5, RD-6].

The present assessment focuses on establishing evidence for the continuity and improvements as compared to the version 6.3. This is achieved by intercomparisons of the former revision and the new revisions to common external references.

1.3 Applicable Documents

Id	Title	Reference
AD-1	EPS Programme End User Requirements Document	EUM/EPS/MIS/REQ/93/001
AD-2	IASI Level 2 Regional Service End-User Requirements	EUM/TSS/REQ/16/846400

1.4 Reference Documents

Id	Title	Reference
RD-1	IASI L2 PPF v6: Validation Report	EUM/TSS/REP/14/776443
RD-2	IASI L2 PPF v6.2: Validation Report	EUM/RSP/REP/16/857500
RD-3	IASI L2 PPF v6.3: Validation Report	EUM/RSP/REP/17/920559
RD-4	"A Global Assessment of NASA AIRS v6 and EUMETSAT IASI v6 Precipitable Water Vapor using Ground-based GPS SuomiNet Stations"	Roman et al., JGR 2016, doi :10.1002/2016JD024806
RD-5	"Identification and intercomparison of surface-based inversions over Antarctica from IASI, ERA-Interim, and Concordiasi dropsonde data"	Boylan et al., JGR 2016, doi :10.1002/2015JD024724
RD-6	"Assessment of NOAA NUCAPS upper air temperature profiles using COSMIC GPS radio occultation and ARM radiosondes"	Feltz et al., JGR 2017, doi :10.1002/2017JD026504
RD-7	OSI-SAF Metop-A IASI Sea Surface Temperature L2P (OSI-208) Validation report, April 2015	SAF/OSI/CDOP2/M-F/TEC/RP/210, v1.4
RD-8	Group for High-Resolution Sea Surface Temperature (GHRSST)	https://www.ghrsst.org/
RD-9	Monitoring & Evaluation of Thematic Information from Space (METIS) – Sea Surface Temperature (SST)	http://metis.eumetsat.int/sst
RD-10	Internal prototype METIS SST monitoring http://tcweb/tcenas/proj/ocean/metis/sst/index_iasi.html#	
RD-11	IASI L2 Product Generation Specifications	EPS.SYS.SPE.990013
RD-12	Algorithm Theoretical Basis Document for Land Surface Temperature, LSA-SAF	SAF/LAND/IM/ATBD_LST/1.0
RD-13	SAF for Land Surface Analysis – Validation Report LST, LSA SAF	SAF/LAND/IM/VR_LST/I_08
RD-14	Product User Manual – Land Surface Temperature, LSA SAF	SAF/LAND/IM/PUM_LST/2.4
RD-15	Borbas et al., "NASA MEaSUREs Combined ASTER and MODIS Emissivity over Land (CAMEL)", American Geophysical Union, Fall General Assembly 2016, abstract #GC51D-1203 University of Winsconsin global database of infrared land surface emissivity from MODIS and ASTER, http://cimss.ssec.wisc.edu/iremis/	
RD-16	ERA-5 http://climate.copernicus.eu/products/climate-reanalysis	
RD-17	Integrated Global Radiosonde Archive (IGRA) database https://www.ncdc.noaa.gov/data-access/weather-balloon/integrated-global-radiosonde-archive	
RD-18	"Retrieval of sulphur dioxide from the infrared atmospheric sounding interferometer (IASI)"	Clarisse et al., AMT 2012, doi:10.5194/amt-5-581-2012
RD-19	"FORLI radiative transfer and retrieval code for IASI"	Hurtmans et al., JQSRT 2012, DOI: 10.1016/j.jqsrt.2012.02.036

RD-20	EARS-IASI Level 2 EUMETSAT Advanced Retransmission Service, Regional Data Service https://www.eumetsat.int/website/home/Data/RegionalDataServiceEARS/EARSIASI/ EARS IASI Level 2 announcement https://www.eumetsat.int/website/home/News/DAT_3709776.html	
RD-21	"Infrared Continental Surface Emissivity Spectra and Skin Temperature Retrieved from IASI Observations over the Tropics"	Capelle V. et al., 2011, Journal Of Applied Meteorology And Climatology, doi: 10.1175/JAMC-D-11-0145.1
RD-22	Report for the EARS-IASI L2 Product Validation Review Board	EUM/RSP/REP/17/904822
RD-23	MonaLisa - Software Release Note	EUM/RSP/TEN/17/930189

1.5 Acronyms

Acronym	***Meaning***
AC SAF	Atmospheric Composition Satellite Application Facility
ANN	Artificial Neural Network
ARM	Atmospheric Radiation Measurement (US program)
AVHRR	Advanced Very High Resolution Radiometer, the imager on-board Metop
CALC	CALCulated - Refers to synthetic radiances calculated with a radiative and an atmospheric state vector which may come from the NWP or the L2.
Cal/Val	Calibration / Validation
ECMWF	European Centre for Medium-Range Weather Forecasts
EPS	EUMETSAT Polar System
EUMETSAT	European Organisation for the Exploitation of Meteorological Satellites
EURD	End User Requirements Document
EOF	Empirical Orthogonal Function
FG	First Guess
GCOS	Global Climate Observing System
GHRSST	Group for High Resolution Sea Surface Temperature
GRUAN	GCOS Reference Upper-Air Network
IASI	Infrared Atmospheric Sounding Interferometer
IASI-A	IASI onboard Metop-A
IASI-B	IASI onboard Metop-B
IFOV	Instantaneous Field Of View
LATMOS	Laboratoire Atmosphères, Milieux, Observations Spatiales (Paris, France)
LSA	Land Surface Analysis
LST	Land Surface Temperature
L2	Level 2
MODIS	Moderate Resolution Imaging Spectroradiometer

MONALiSA	MONitoring of Atmospheric Level2 SAtellite products
MWR	Microware radiometer
NOAA	National Oceanic and Atmospheric Administration (US)
NPROVS	NOAA Products Validation System
NRT	Near-Real Time
NWP	Numerical Weather Prediction
OBS	Observations (usually refers to L1c radiances)
OEM	Optimal Estimation Method
OSI SAF	Ocean and Sea Ice Satellite Application Facility
PC	Principal Components
PPF	Product Processing Facility
PWV	Precipitable Water Vapour
PWLR	Piecewise Linear Regression
$PWLR^3$	Piecewise Linear Regression-cube
RMS	Root Mean Square
SAF	Satellite Application Facility
SEVIRI	Spinning Enhanced Visible and Infrared Imager
SST	Sea Surface Temperature
ULB	Université Libre de Bruxelles
UTC	Coordinated Universal Time

2 PROCESSOR CHANGES AND VALIDATION DATA DESCRIPTION

2.1 IASI L2 processor overview

The Figure 1 recalls the main steps of the IASI L2 operational processor. Firstly, the IASI L1c spectra are compressed into principal component scores. Auxiliary information from static atlases (e.g. digital elevation model, land/sea atlas…) and dynamic inputs (e.g. microwave measurements from AMSU and MHS companion instruments) are collocated to the IASI pixels. It is worth noting that no NWP forecasts are used in the subsequent atmospheric retrievals, with the exception of the AC SAF libraries which may use forecasts in the absence of retrievals from IASI (e.g. with certain thick clouds).

The first retrieval is based on a statistical method, namely the PWLR^3 which stands for piece-wise linear regression –cube. It exploits IASI infrared (IR) and AMSU/MHS microwave (MW) measurements in synergy in nominal conditions. It includes an IR-only fall-back mode in the absence of suitable microwave information. The first atmospheric retrieval is followed by a cloud detection and characterisation. In cloud-free pixels, the temperature, humidity and ozone products are refined with an optimal estimation method (OEM), which uses the PWLR^3 first retrieval as *a priori*. The last step is dedicated to the EUMETSAT AC SAF atmospheric composition and air quality products, generated with the FORLI [RD-19] and BRESCIA [RD-18] libraries developed at ULB and LATMOS.

The reader is referred to the IASI L2 Product Generation Specifications [RD-11] for a detailed description of the processing algorithms and products.

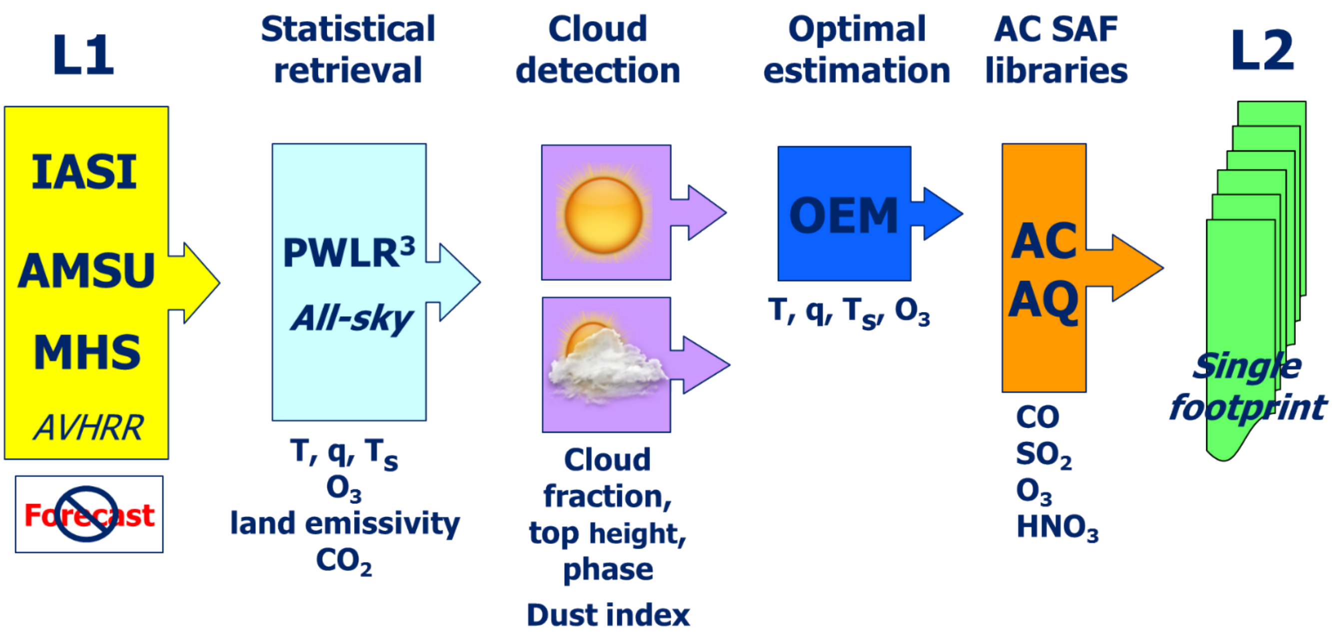

Figure 1: IASI L2 processing sequence

2.2 Algorithms and products updates

The initial main motivations for the revision 6.4 were:

- A small increasing bias in the tropospheric temperature as the CO_2 static configuration of RTTOV in v6.3 (~380 ppmv) has become outdated because of the CO_2 rise. RTTOV in v6.4 is configured with the latest coefficients, including contemporary CO_2 concentrations.
- To improve the IR-only fall-back mode (in the absence of MW data) of the first retrieval with the statistical method PWLR[3] (PieceWise Linear Regression –cube).

In addition, an anomaly in the quality control of the SST L2Pcore products was reported about v6.3 products during the qualification of the v6.4. The v6.4 was then patched with an updated quality control algorithm.

A few other enhancements have been included, which are summarised in the following table.

Processing function	Short description of the changes in v6.4	Parameters impacted
First retrieval (PWLR[3])	Enhanced 'all-sky' first retrieval with better clustering of the observations and training sets (ERA-5 [RD-16] for T, q, O_3, T_s), CAMEL [RD-15] for land surface emissivity. Largest improvement with the IR-only mode (when AMSU/MHS data not available), with benefits also to the nominal combined MW+IR retrieval. Updates to the quality indicators	All-sky first-guess, e.g.: - Temperature - Humidity - Land surface emissivity - Quality indicators
OEM	Updated RTTOV coefficients with contemporary CO_2 concentrations (~400ppmv), to account for CO_2 rise. This reduces a small bias in tropospheric temperature which resulted from slightly outdated CO_2 configuration in previous IASI L2 versions.	Clear-sky final: - Temperature - Humidity
SST L2Pcore	Refined the quality control and assignment in quality classes. The SST precision is slightly enhanced as a result of the above first retrieval and OEM updates. Bug fix: stop time of SST L2Pcore files now set to stop time of last record (instead of start time of last record)	SST L2Pcore quality classification
SO_2	Bug fix: one 3' granule lost in 8 months because of executable crash in the BRESCIA library	EUM AC SAF IASI SO2 availability
Product flags	Bug fix: the flag FLG_INITIA records the origin of the measurements in the first retrieval (IASI, AMSU, MHS)	FLG_INITIA
Product header record	Bug fix: Main Product Header Record (MPHR) includes L1C parent product filename	MPHR

2.3 Processor versioning

The version intended for roll-out on GS1 is the v6.4.4. The results presented in this report were obtained from off-line processing on the Technical and Computing Environment (TCE) of EUMETSAT and from routine production on the validation ground segment (GS2) since the first release of v6.4.1 on 21/12/2017. Intermediate patches were made to resolve minor bugs, with no impact on the core scientific product validation and were not rolled out on GS2. The version v6.4.4 was deployed on GS2 on 25/01/2018 to include the patch to the L2Pcore SST quality control.

Both Metop-A and Metop–B products are evaluated separately in this document, to demonstrate their consistency.

2.4 Assessment of temperature and humidity with radiosondes

Radiosondes provide *in situ* atmospheric measurements and have been coordinated in a global international effort to supply information at synoptic times for assimilation in the numerical weather prediction models. They also constitute independent reference data which are very valuable for the validation of satellite products. As the atmosphere is varying in space and time, collocation errors may account for an important part of the uncertainty budget when assessing satellite products against radiosondes, especially for tropospheric humidity. In this work, the match-up criteria allow for a maximum of 3 hours difference in time and 50 km in space between IASI observations and the sonde release.

A monitoring facility –aka MONALiSA, MONitoring of Atmospheric Level2 SAtellite products - has been developed at EUMETSAT, with the goal to perform continuous collocation, comparison and statistics between *in situ* sonde measurements and IASI L2 profiles. It collocates sonde measurement pre-processed at NOAA and released on a daily basis in the IGRA database [RD-17]. MONALiSA compiles statistics of sonde vs satellite profiles either globally or in user-configurable geographical areas. Auxiliary information such as quality indicators, land/sea, cloud flags are used to stratify the analysis. MONALiSA can be scheduled to update the statistics on a daily basis and offers the possibility of automated reporting in graphic files. These typically include:

- vertical profiles of bias and standard deviation of difference IASI vs sondes
- maps of biases and standard deviation in selected layers
- time series of bias, standard deviation, match-up size at configurable pressure levels

In this work as well as in the comparison to model analyses, the satellite and reference profiles are compared point-to-point in the vertical, without accounting for their respective vertical sensitivity, e.g. by application of averaging kernels or by slab-layering. The IGRA profiles do not contain the full sonde resolution as they are provided at a limited number of significant levels. Such a scientific work including satellite products vertical sensitivity (e.g. with averaging kernels) was systematic performed during the commissioning of Metop-B and for the qualification of the first IASI L2 v6 release. The approach here with direct level-to-level comparison is sufficient to monitor and characterise some potential improvements in the sounding precision and to perform the necessary non-regression checks with the introduction of the new version.

2.5 Stratification of comparisons to ECMWF analyses

Temperature and humidity are compared to the analyses of ECMWF numerical model [00, 06, 12 and 18 UTC], interpolated in space and time to the IASI observations. This enables large statistics with global coverage, which are useful to perform non-regression checks *vs* the former processor version and to provide a first indications of the sounding performances as well as possible regional variations. The validation of the temperature and humidity profiles is performed by comparison and monitoring against *in situ* radiosondes (see §2.4).
The comparisons to ECMWF are performed globally and the statistics presented in this document are stratified against the following reference geographic classes.

Class	*Label*	*Surface pressure*	*Surface type*	*Latitude*	*Time*
1	North Polar cap	< 1050 hPa	land and sea	> 60°	day and night
2	North Sea	> 900 hPa	sea	[30° ; 60°]	day and night
3	North Land	> 900 hPa	land	[30° ; 60°]	day and night
4	High Elevation	< 900 hPa	land	[–60° ; 60°]	day and night
5	Intertropic Sea	> 900 hPa	sea	[–30° ; 30°]	day and night
6	Intertropic Land	> 900 hPa	land	[–30° ; 30°]	day and night
7	South Polar cap	< 1050 hPa	land and sea	< -60°	day and night
8	South Sea	> 900 hPa	sea	[–60° ; 30°]	day and night
9	South Land	> 900 hPa	land	[–60° ; 30°]	day and night

Table 1: Definition of the validation geographic classes

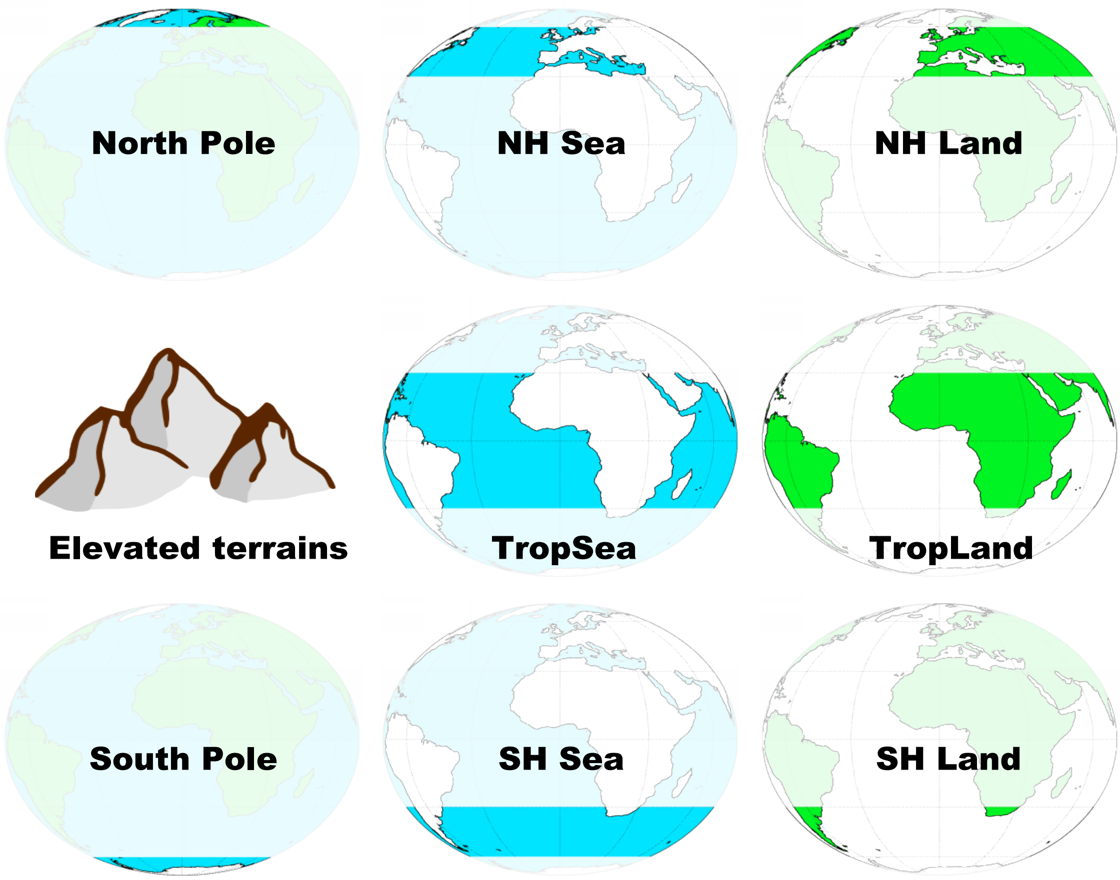

Figure 2: Geographic classes used in the IASI L2 validation

3 PWLR^3: FIRST RETRIEVAL OF TEMPERATURE AND HUMIDITY PROFILES

The first retrieval function of the IASI L2 central processor is the PWLR^3 (piece-wise linear regression –cube), which generates temperature and humidity profiles, among other geophysical parameters, in nearly all-sky conditions. The regional service EARS-IASI L2 [RD-20] operates the same retrieval PWLR^3 function as in the central global processing.

In its nominal mode, the PWLR^3 jointly exploits IASI spectra with collocated microwave measurements from AMSU and MHS. It is referred to as MW+IR mode. The infrared-only mode (IR-only) is the fall-back configuration in the absence of suitable collocated microwave information, whereby only IASI information is exploited. It is expected to be more affected by clouds than the MW+IR.

Temperature and humidity profiles retrievals were reprocessed off-line in the two modes (IR-only and MW+IR) from January 2017 to October 2017 and compared to IGRA radiosonde *in situ* measurements. The results presented in the sections 3.1 and 3.2 were computed with the best 50% retrievals, i.e. in cloud-free pixels and pixels partly affected by clouds. A stratification of this intercomparison based on the quality indicator for temperature is presented in section 3.3.

3.1 Comparison of reprocessed IR-only PWLR³ retrievals to radiosondes

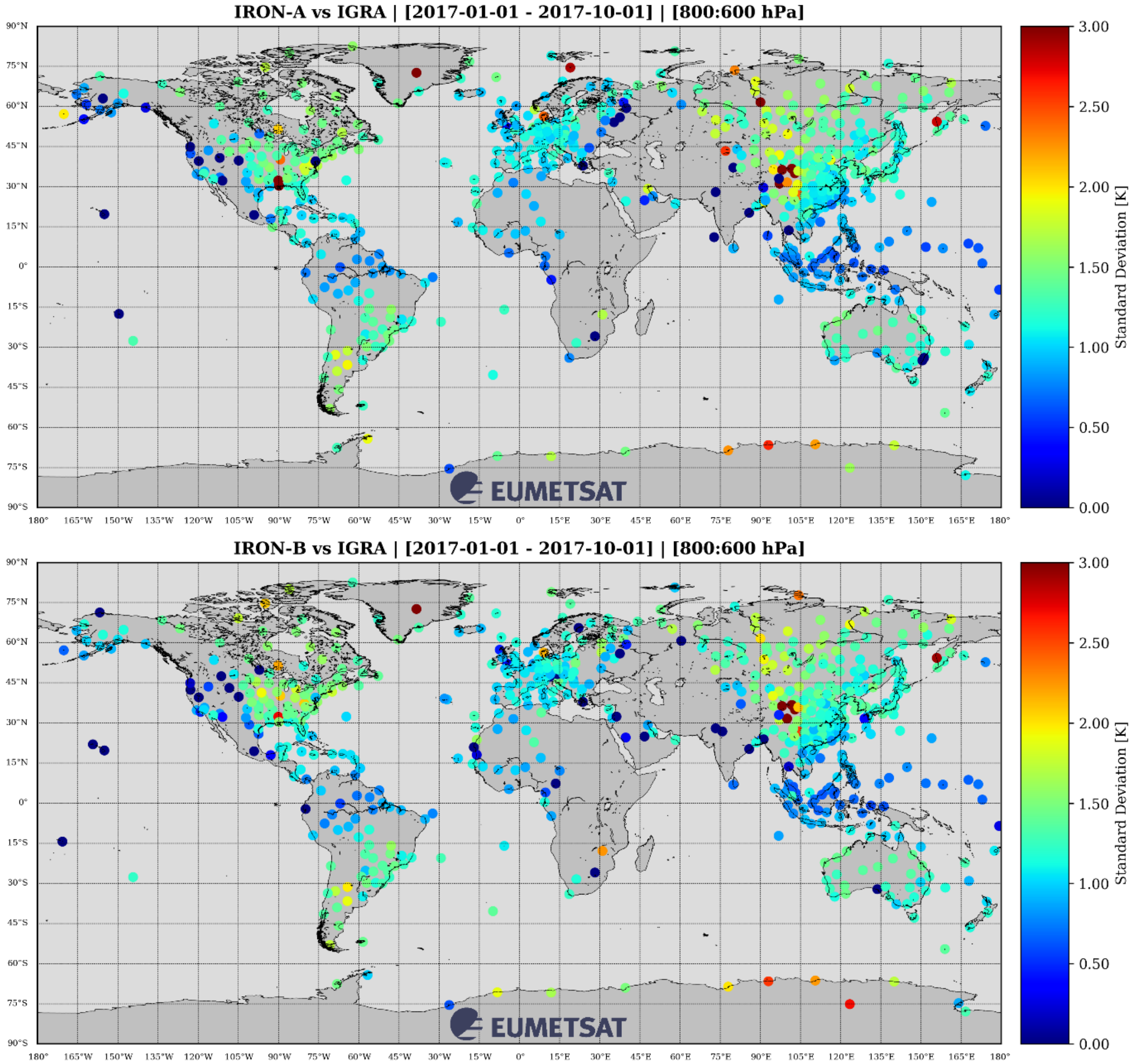

Figure 3: Standard deviation of the temperature difference between sonde measurements and IR-only PWLR³ retrievals from IASI-A (top) and IASI-B (bottom) in the 600-800 hPa layer between January and October 2017.

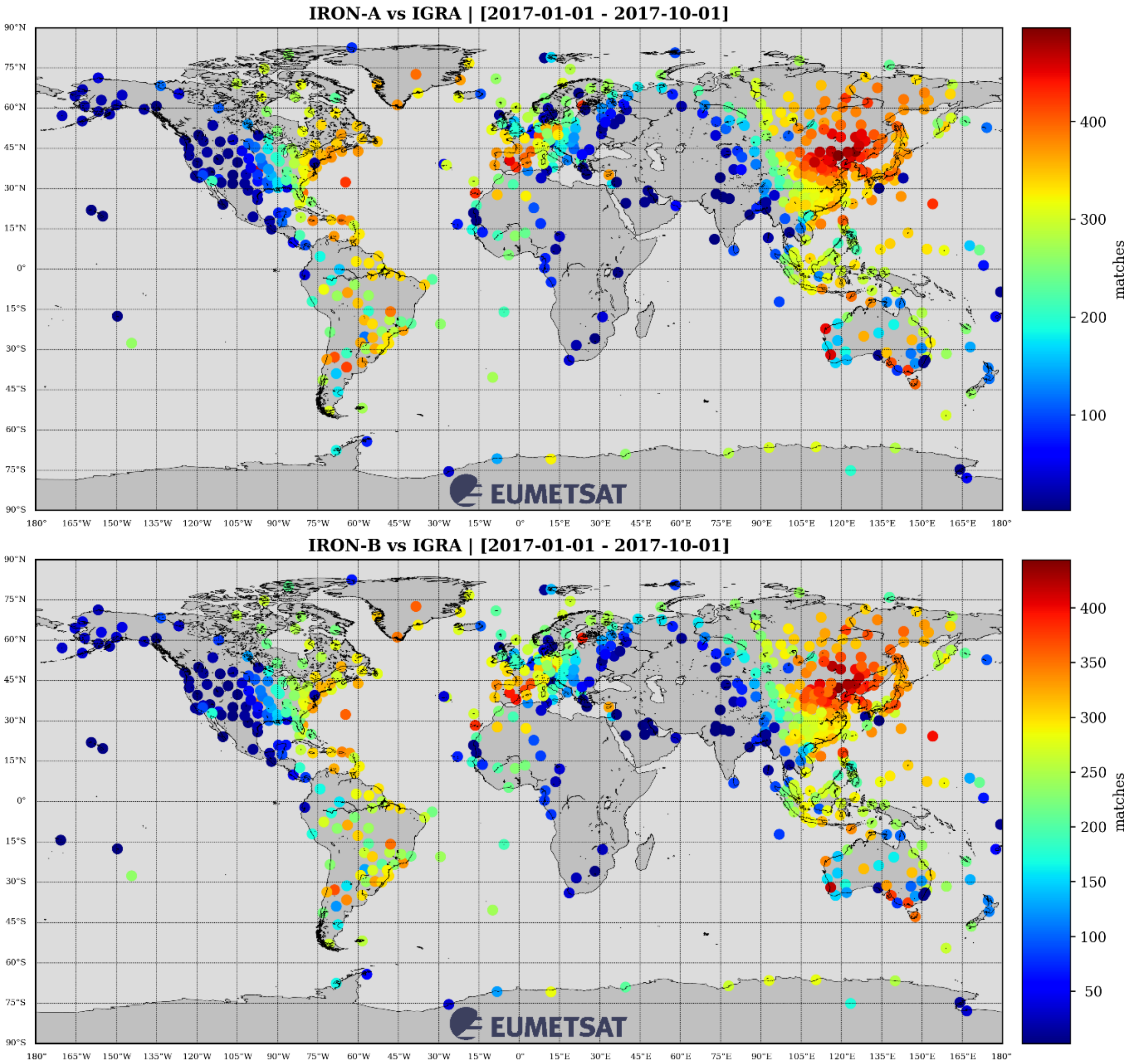

Figure 4: Match-up counts at each sonde site with the IR-only PWLR³ retrievals from IASI-A (top) and IASI-B (bottom) between January and October 2017.

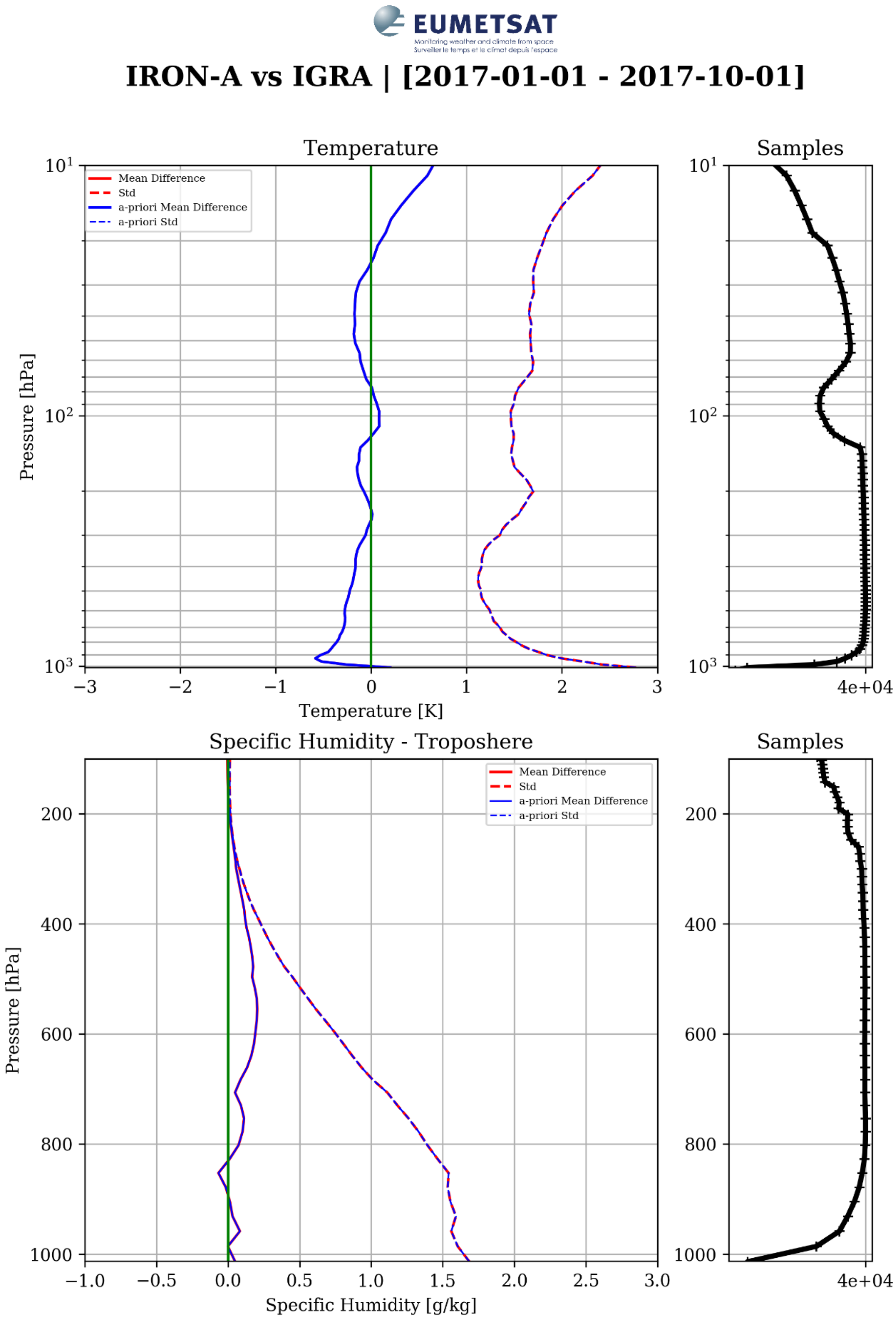

Figure 5: Differences (solid: bias, dash: standard deviation) between radiosonde measurements and IR-only PWLR[3] retrievals from Metop-A in temperature (top) and humidity (bottom), January to October 2017.

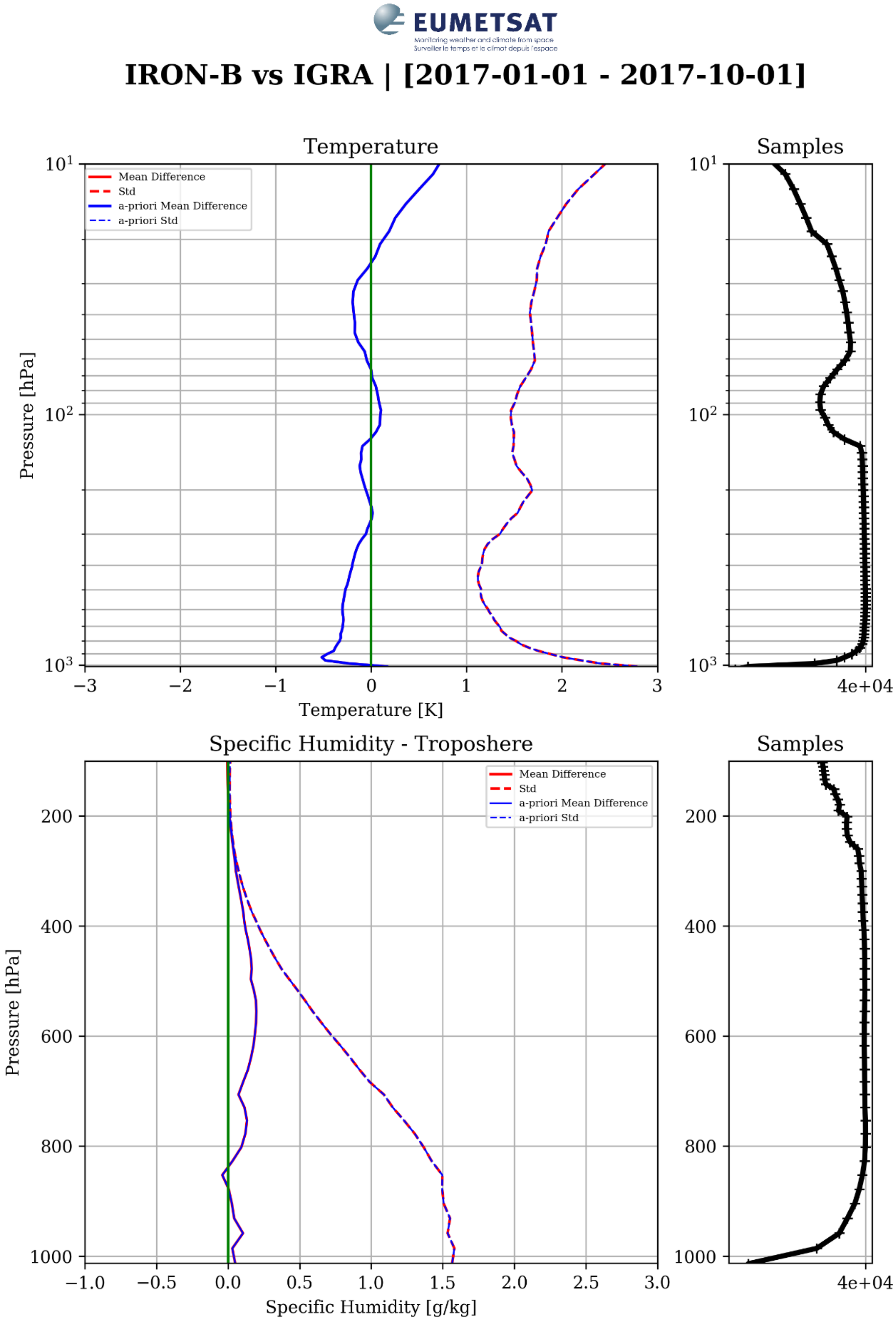

Figure 6: Same as previous, for Metop-B.

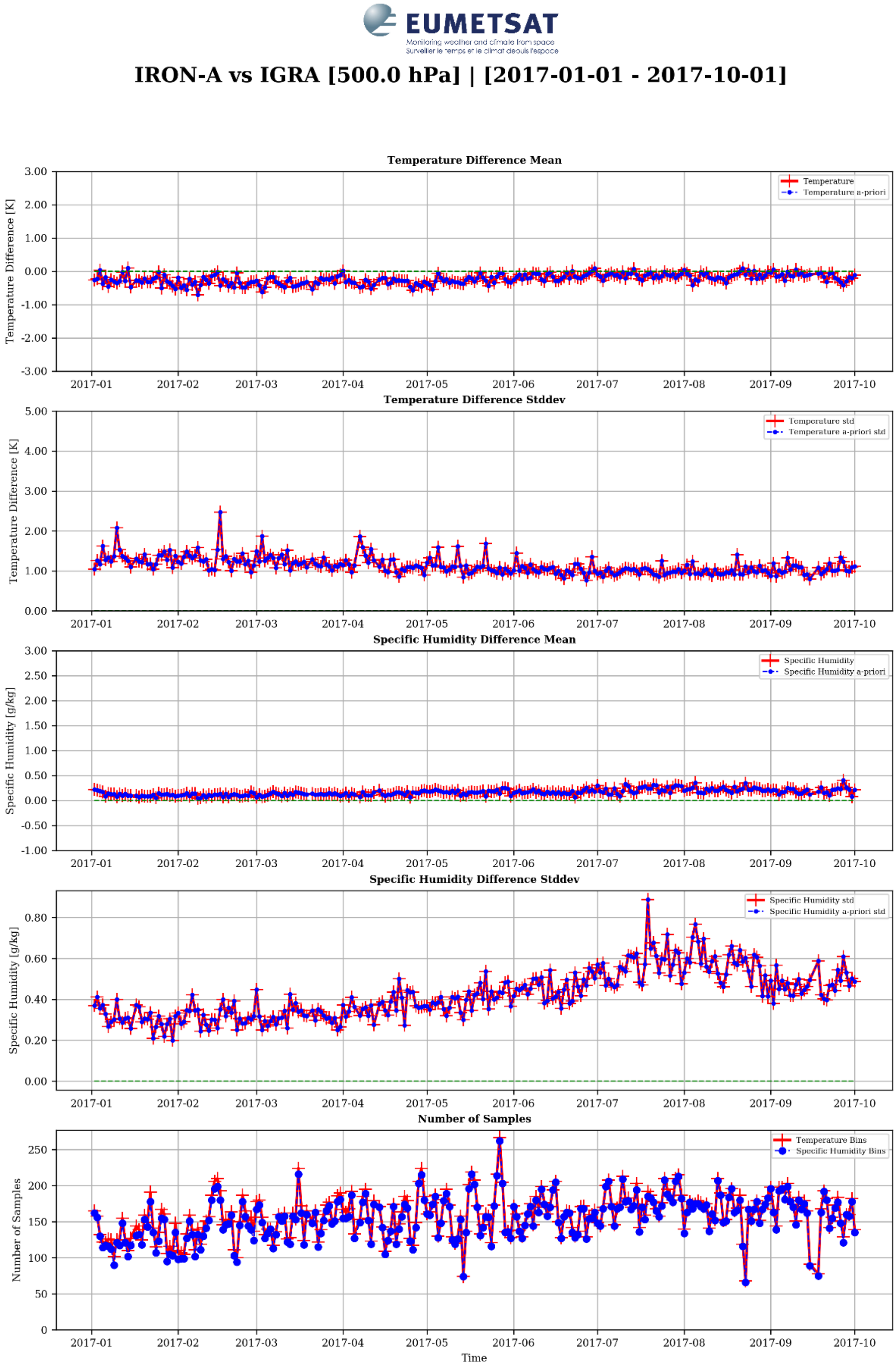

Figure 7: Time series of temperature and humidity differences between IR-only PWLR[3] retrievals from Metop-A and radiosondes at 500 hPa, from January to October 2017.

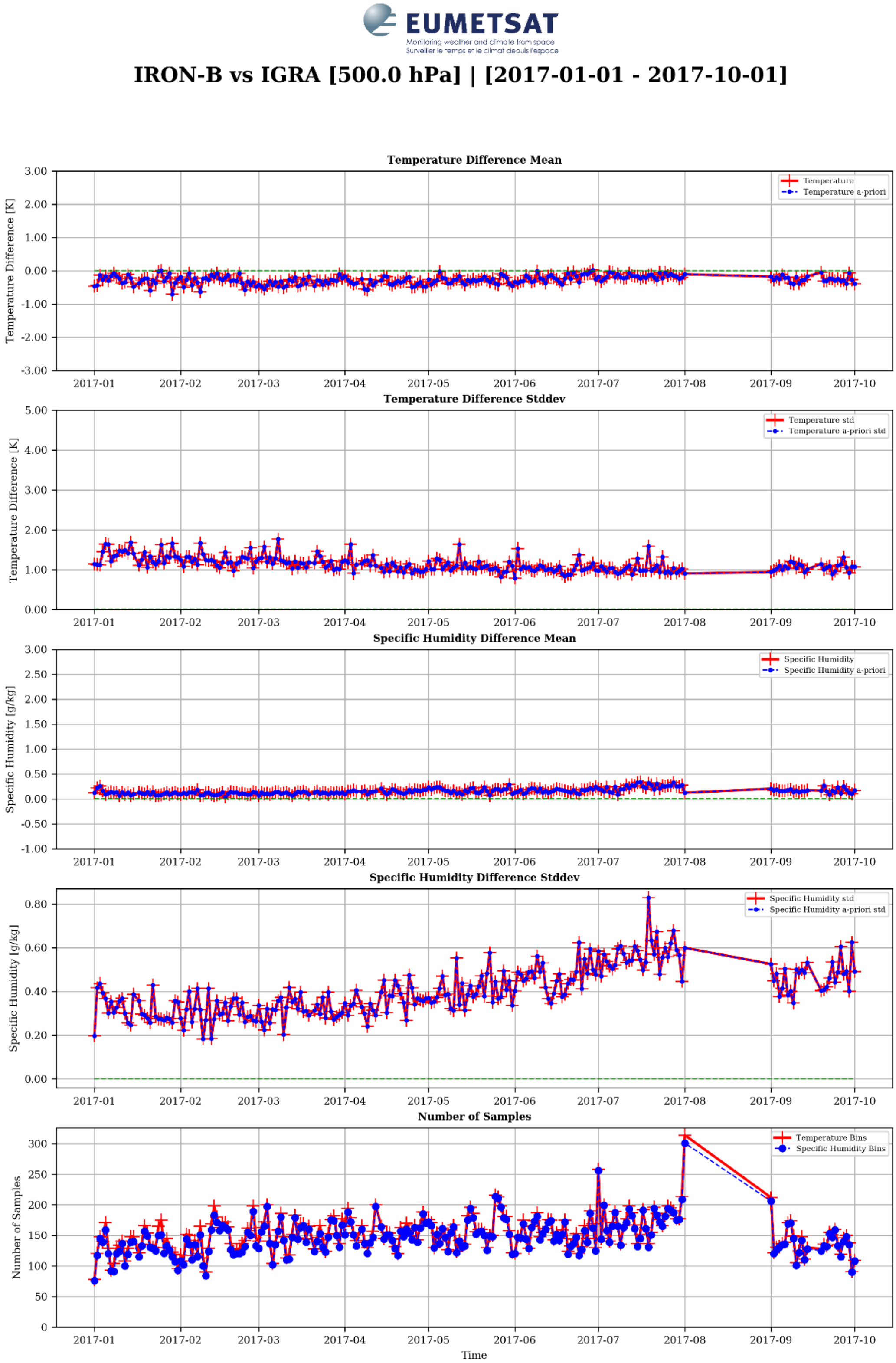

Figure 8: Same as previous, for Metop-B.

3.2 Comparison of reprocessed MW+IR PWLR^3 retrievals to radiosondes

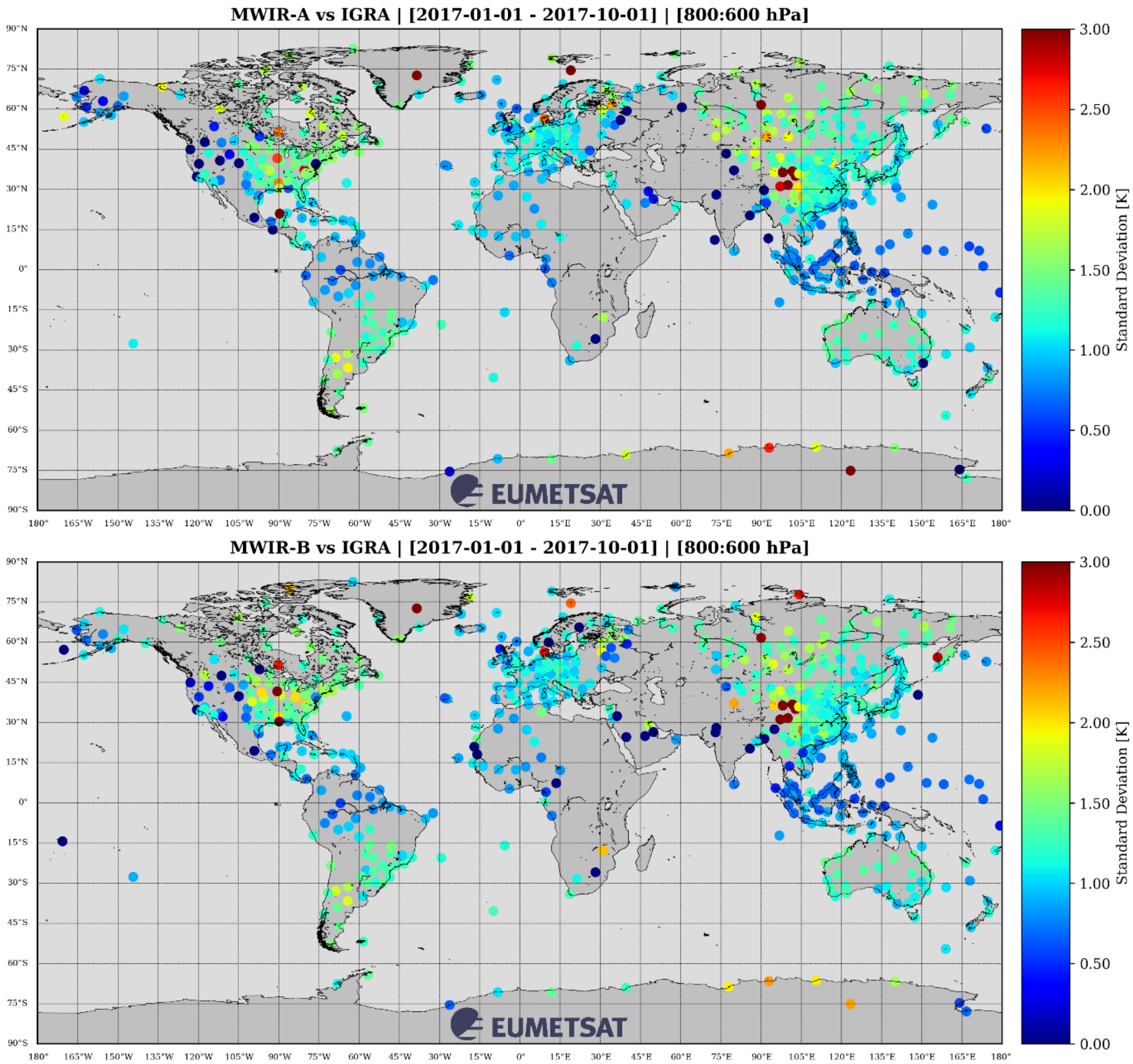

Figure 9: Standard deviation of the temperature difference between sonde measurements and MW+IR PWLR^3 retrievals from IASI-A (top) and IASI-B (bottom) in the 600-800 hPa layer between January and October 2017.

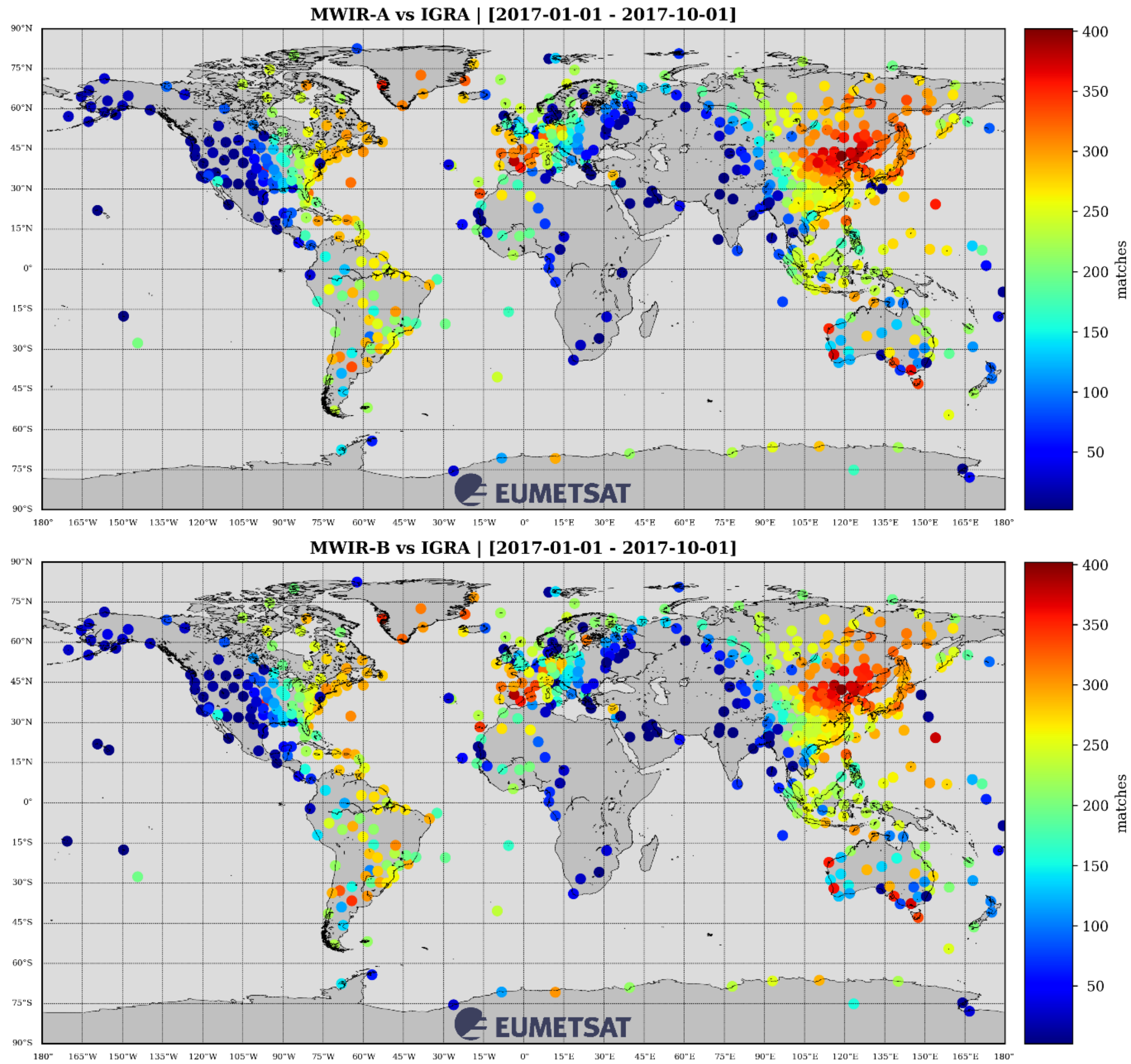

Figure 10: Match-up counts of sonde collocations with the MW+IR PWLR³ retrievals from IASI-A (top) and IASI-B (bottom) between January and October 2017.

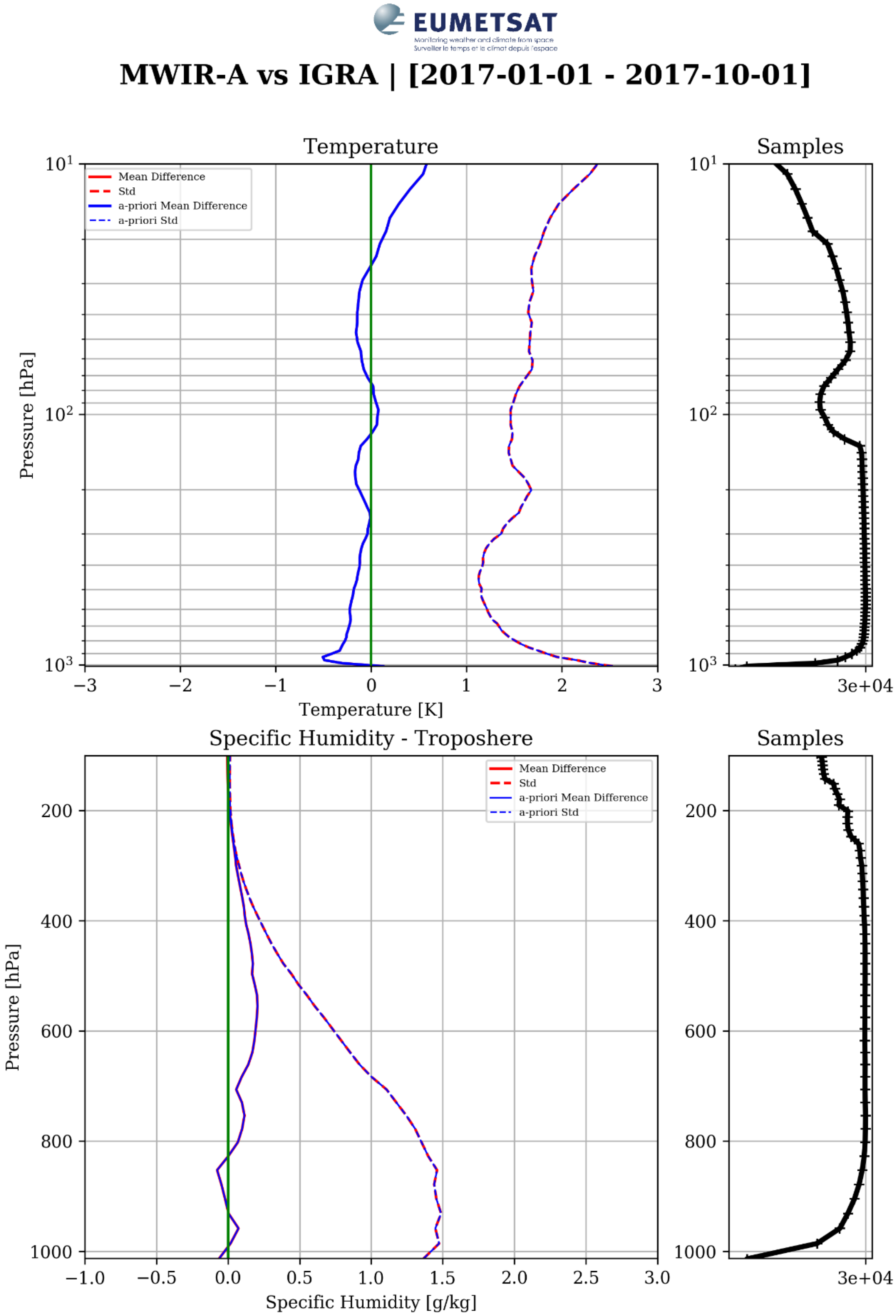

Figure 11: Differences (solid: bias, dash: standard deviation) between radiosonde measurements and MW+IR PWLR[3] retrievals from Metop-A in temperature (top) and humidity (bottom), January to October 2017.

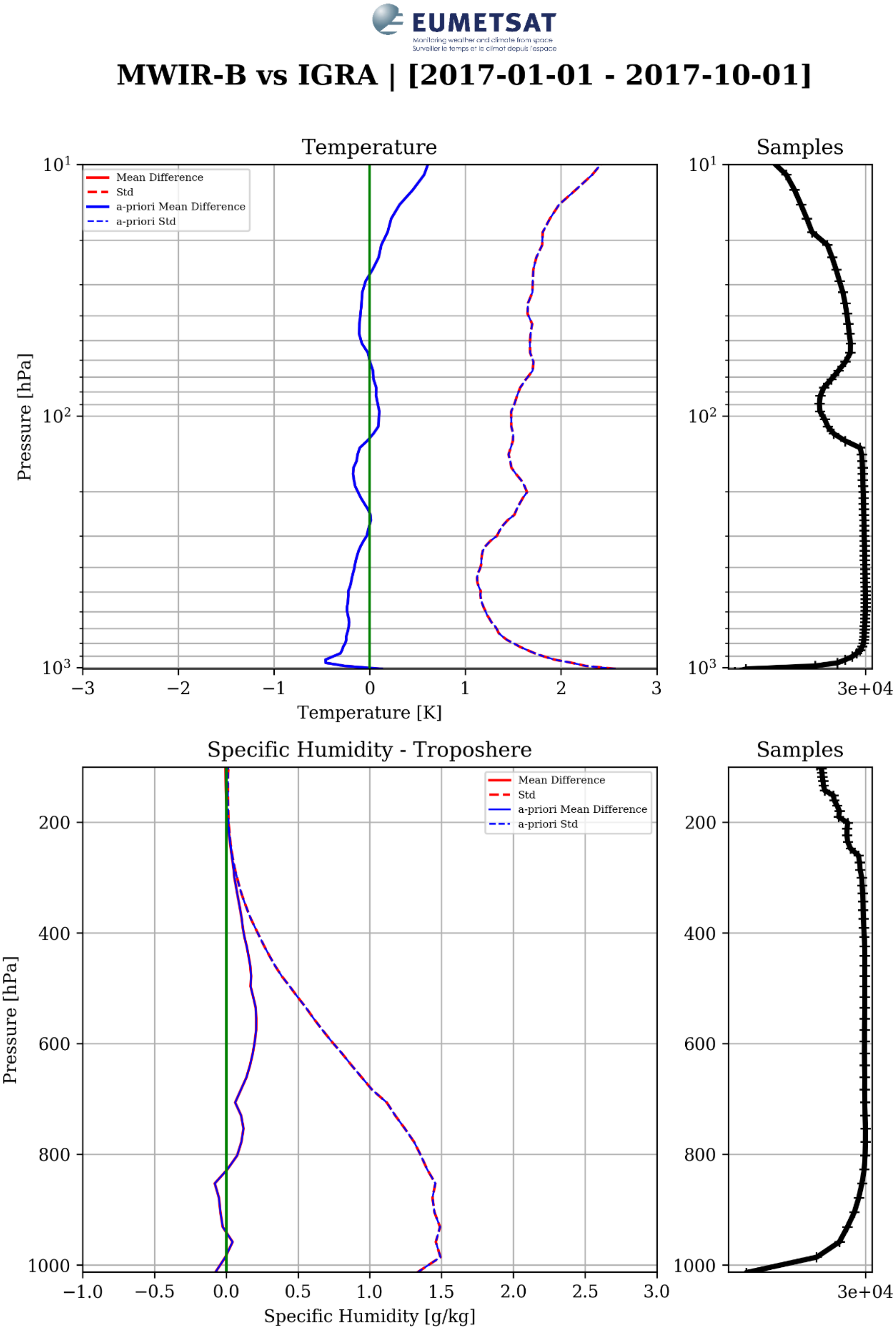

Figure 12: Same as previous, from Metop-B

3.3 Assessment of the quality indicator for temperature with radiosondes

With the PWLR[3], the geophysical parameters are retrieved together with corresponding quality indicators, which are uncertainty estimates. In the case of temperature, the quality indicator from the PWRL[3] is an uncertainty estimate in the lower troposphere, expressed in K.
To evaluate its significance, the statistics (IASI L2 *minus* sondes) were stratified in different bins with that quality indicator. The Figure 13 shows the statistics obtained for Metop-A in the IR-only (left) and in the MW+IR (right) modes. The bias (plain lines) and standard deviations (dash lines) are plotted for five consecutive intervals of the quality indicator for temperature. The relative sample size are represented in the Figure 14 for IR-only (left) and MW+IR (right), with the same colour-code, as follows:

- 0 .. 0.75 Kin black
- 0.75 .. 1 Kin blue
- 1 .. 1.5 K in green
- 1.5 .. 2 K in yellow
- > 2 K in red

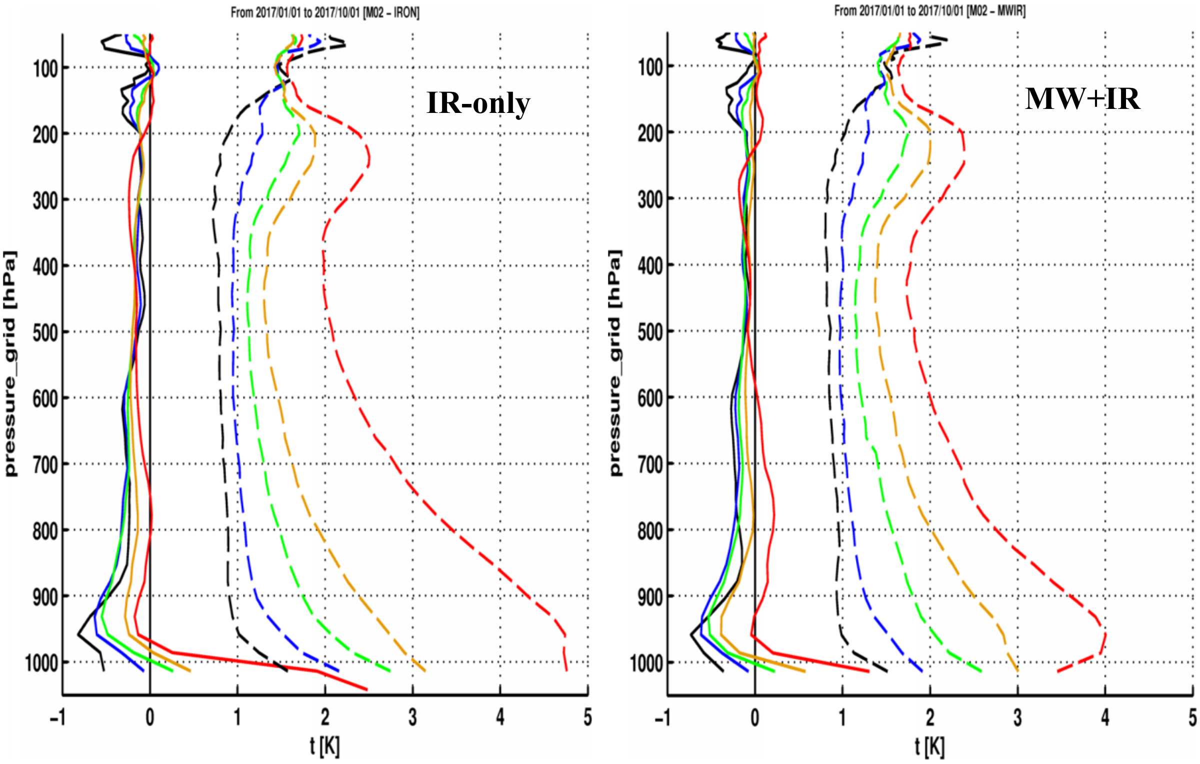

Figure 13: Differences between IASI PWLR³ temperature (left: IR-only, right: MW+IR) and radiosondes, stratified with the quality indicator for temperature, from January to October 2017.

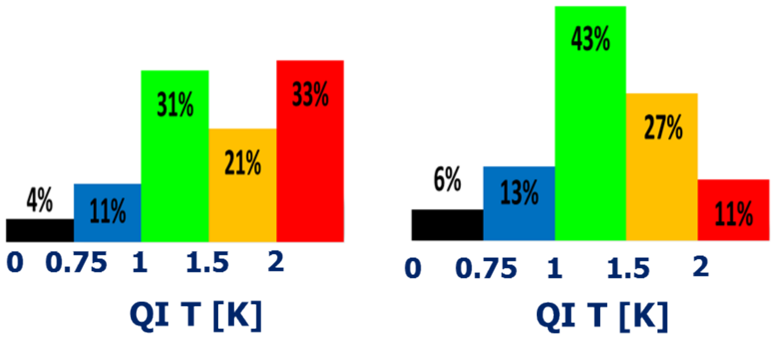

Figure 14: Relative sample size of the five quality classes for temperature, with the IR-only (left) and MW+IR (right) retrievals.

The coverage and distribution of the match-ups is illustrated in the Figure 15, which shows the standard deviation of the (IASI *minus* sonde) differences in the atmospheric layer 600-800 hPa in the different quality intervals, between January and October 2017. It can be seen that for a vast majority, the match-ups are located in the continental surface, mostly in the Northern Hemisphere. A few stations systematically present large departures, notably in China, in the Arctic and also on the Antarctic coasts. The reasons are not fully known at this stage, further in-depth analysis and quality control of the match-ups will be carried out for routine monitoring.

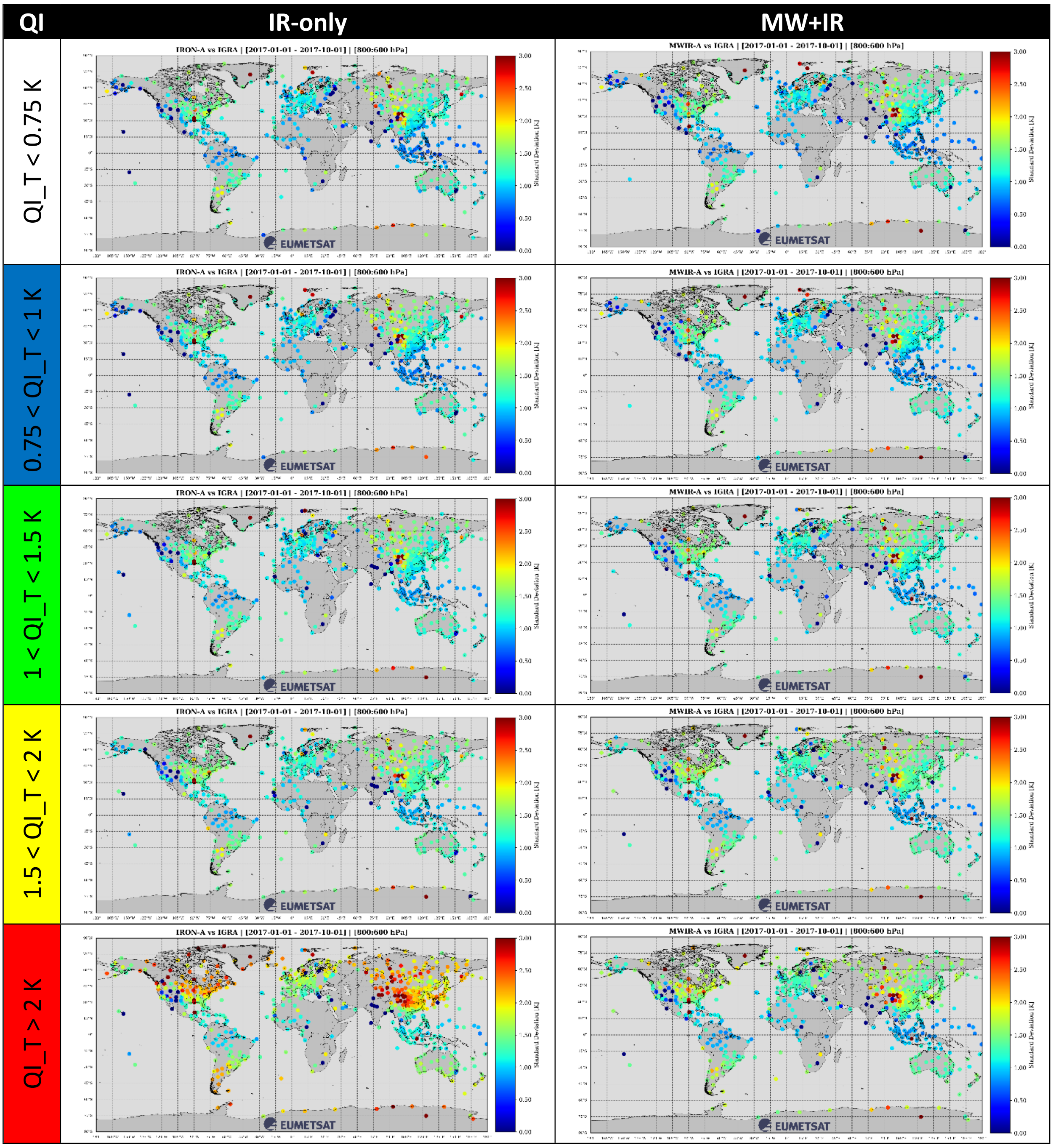

Figure 15: Maps of the standard deviation (IASI temperature vs sondes) in the layer 600-800 hPa with the IR-only (left) and MW+IR (right) modes for the five quality classes defined in Figure 3

4 OEM RETRIEVALS WITH UPDATED RTTOV COEFFICIENTS

It is recalled that retrievals with the optimal estimation method exploit IASI observations only and are exclusively attempted in cloud-free pixels (i.e. FLG_CLDNES equal 1 or 2). The PWLR^3 first retrieval initialises the OEM.

In the v6.4 release, the RTTOV coefficients are the latest-to-date from NWP SAF, including contemporary CO_2 concentrations, while the coefficients used until the v6.3 have slightly outdated (underestimated) CO_2 content compared to nowadays concentrations. We compare hereafter the first (PWLR^3) and second (OEM) retrievals in cloud-free pixels with radiosondes and with ECMWF analysis as described in sections 2.4 and 2.5, respectively. The intercomparisons were performed with products generated with the former (v6.3) and the new (v6.4) versions of the IASI L2 PPF, respectively running on the operational and validation ground segments (namely GS1 and GS2).

4.1 v6.3 and v6.4 temperature profiles vs radiosondes

The period of the intercomparisons extends between 23 December 2017 and 13 February 2018, using correlative sonde measurements (§2.4) within 3 hours and 50 km from the Metop overpass times over Europe. The distribution of the match-ups is illustrated in the Figure 16, which also shows the standard deviation of IASI-sonde temperature in the atmospheric layer 600 to 800 hPa.

The vertical statistics for temperature profiles are summarised in Figure 17 for Metop-A and Metop-B separately, with bias in plain line and standard deviation of the IASI – sonde differences in dash line. The statistics related to v6.4 first retrieval (PWLR^3) and second retrieval (OEM) are displayed in orange and red, respectively. The statistics of PWLR^3 and OEM for v6.3 are displayed in cyan and blue, respectively. The bias is significantly reduced everywhere in the troposphere, except for the very first surface levels. In the mid troposphere the bias has decreased by 0.3 to 0.5 K and now ranges between 0 and 0.3 K with v6.4, except around 500 hPa with Metop-B where the bias with v6.4 reaches 0.5 K but is consistently still smaller than with v6.3. The bias is also improved and closely oscillating around 0 between 100 and 200 hPa with v6.4, but the precision has decreased by 0.2 K in these levels with Metop-A as compared to v6.3. The precision reached with v6.4 and v6.3 are in general comparable, with a slight improvement by about 0.1 K between 700 and 900 hPa with the optimal estimation of v6.4. In general the OEM with v6.4 is comparable to slightly more precise the first statistical retrieval.

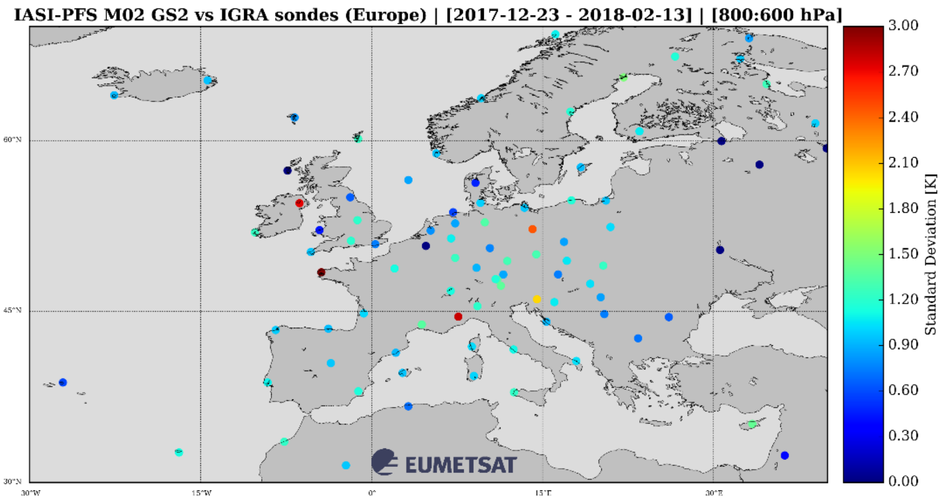

Figure 16: Standard deviation of the temperature difference between sonde measurements and OEM retrievals from IASI-A in the 600-800 hPa layer between 23/12/2017 and 13/02/2018.

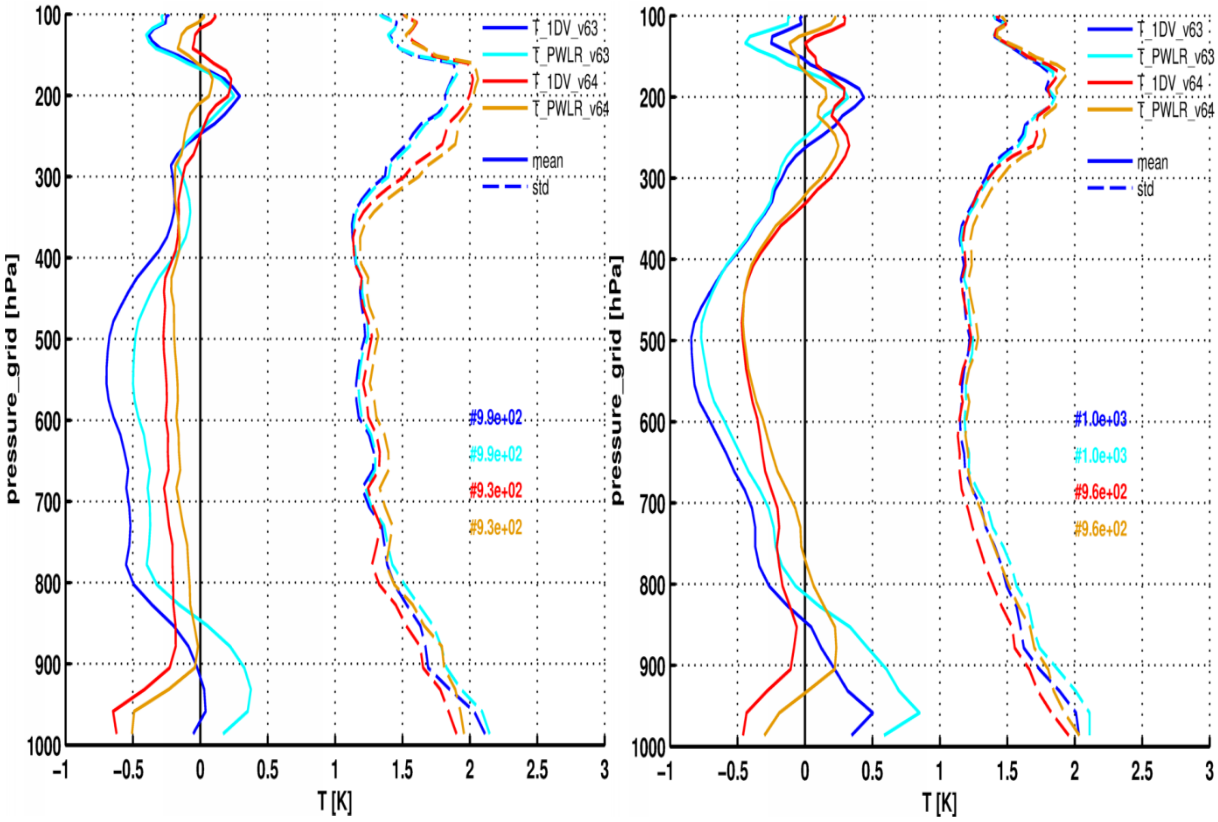

Figure 17: Metop-A (left) and Metop-B (right) temperature retrievals compared to radiosondes between 23 December 2017 and 13 February 2018 with the processor v6.3 (cyan: PWLR[3], blue: OEM) and v6.4 (orange: PWLR[3], red:OEM)

4.2 v6.3 and v6.4 humidity profiles vs radiosondes

The water-vapour profiles retrievals from Metop-A were similary compared to *in situ* sonde measurements as done for temperature in the previous section. The vertical statistics are summarised in Figure 18. Humidity as retrieved with v6.4 is more precise by 0.1 to 0.2 g/kg below 700 hPa. The bias is significantly improved below 800 hPa with v6.4 from Metop-B, by 0.3 to 0.5 g/kg. On the contrary, around 900 hPa, the retrievals seem slightly dry-biased by 0.1 to

0.2 g/kg now with v6.4 on Metop-A. These small differences observed between Metop-A and –B will require further investigations. Overall, as was the case with v6.3 already, the OEM retrieval seems slightly more accurate (bias) and precise (standard deviation) than the PWLR[3] below 700 hPa, by up to 0.1g/kg.

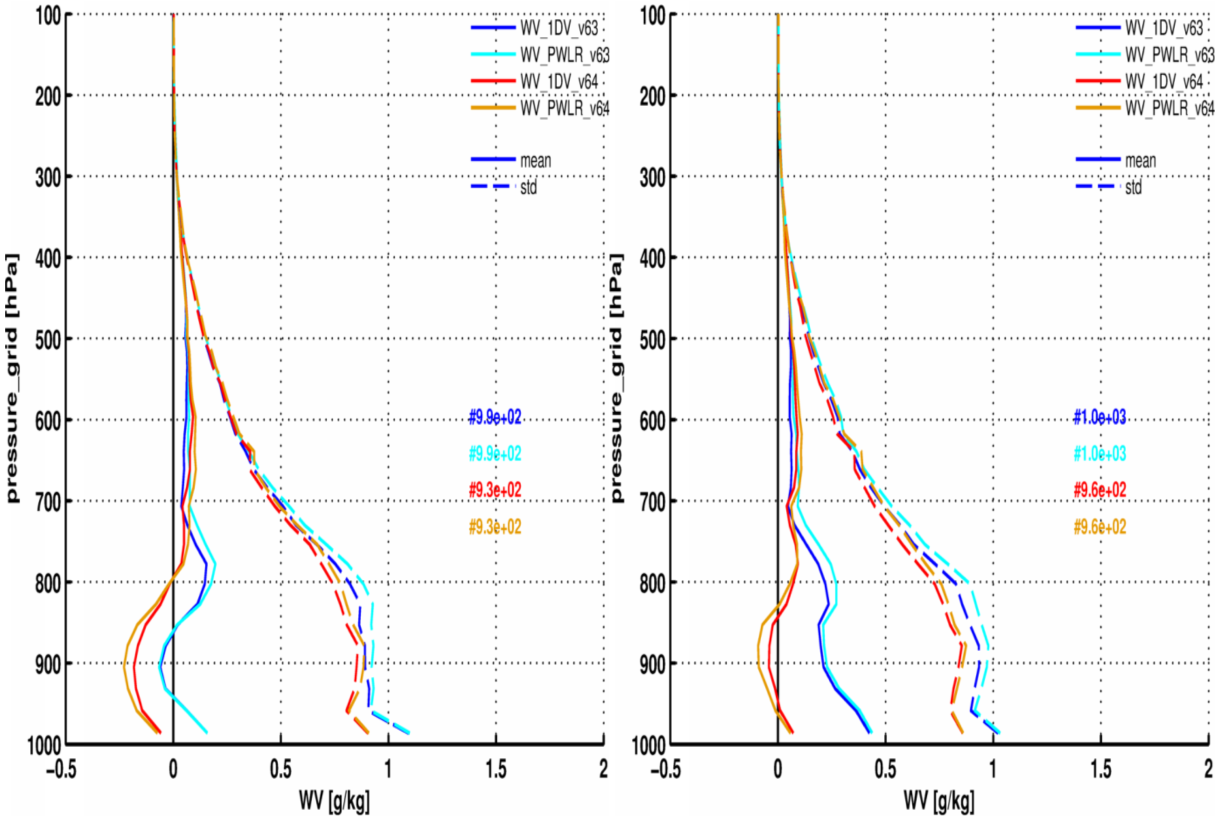

Figure 18: Metop-A (left) and Metop-B (right) temperature retrievals compared to radiosondes between 23 December 2017 and 13 February 2018 with the processor v6.3 (cyan: PWLR[3], blue: OEM) and v6.4 (orange: PWLR[3], red:OEM)

4.3 v6.3 and v6.4 temperature profiles vs ECMWF analysis

The temperature products were compared to ECMWF analysis to allow global coverage and perform a stratification in land/sea and regional classes with statistically significant sample size, as explained in section 2.5. The statistics are summarised in the Figure 19 and Figure 20. Noteworthy, the biases characterised against the model analyses are significantly improved with v6.4. They are flatter and oscillating more closely around 0 K throughout the troposphere than the biases with v6.3 which could be as high as 0.5 K in the mid-troposphere in all regional classes. The observations are consistently applicable to Metop-A and Metop-B products, generated with the PWLR[3] or the OEM. While still improving over v6.3, the biases with v6.4 reach 0.4 to 0.5 K in some mid-tropospheric levels over Northern continental surfaces, which will require further investigations. Interestingly, the biases assessed *vs* sondes did not come up as high. From a precision (standard deviation) point of view, both v6.4 PWLR[3] and OEM present similar to better performances than v6.3 in all regional classes. The best fits are observed in the mid-troposphere with precision as high as 0.6 to 0.7 K. The departures IASI – analyses increase in the boundary layer, from typically 1-1.5 K over oceans to 2 K over land. In general, the OEM is of comparable precision as the PWLR[3] in the upper troposphere and improves by up to 0.1 K in some regions – especially over land- compared to the first retrieval.

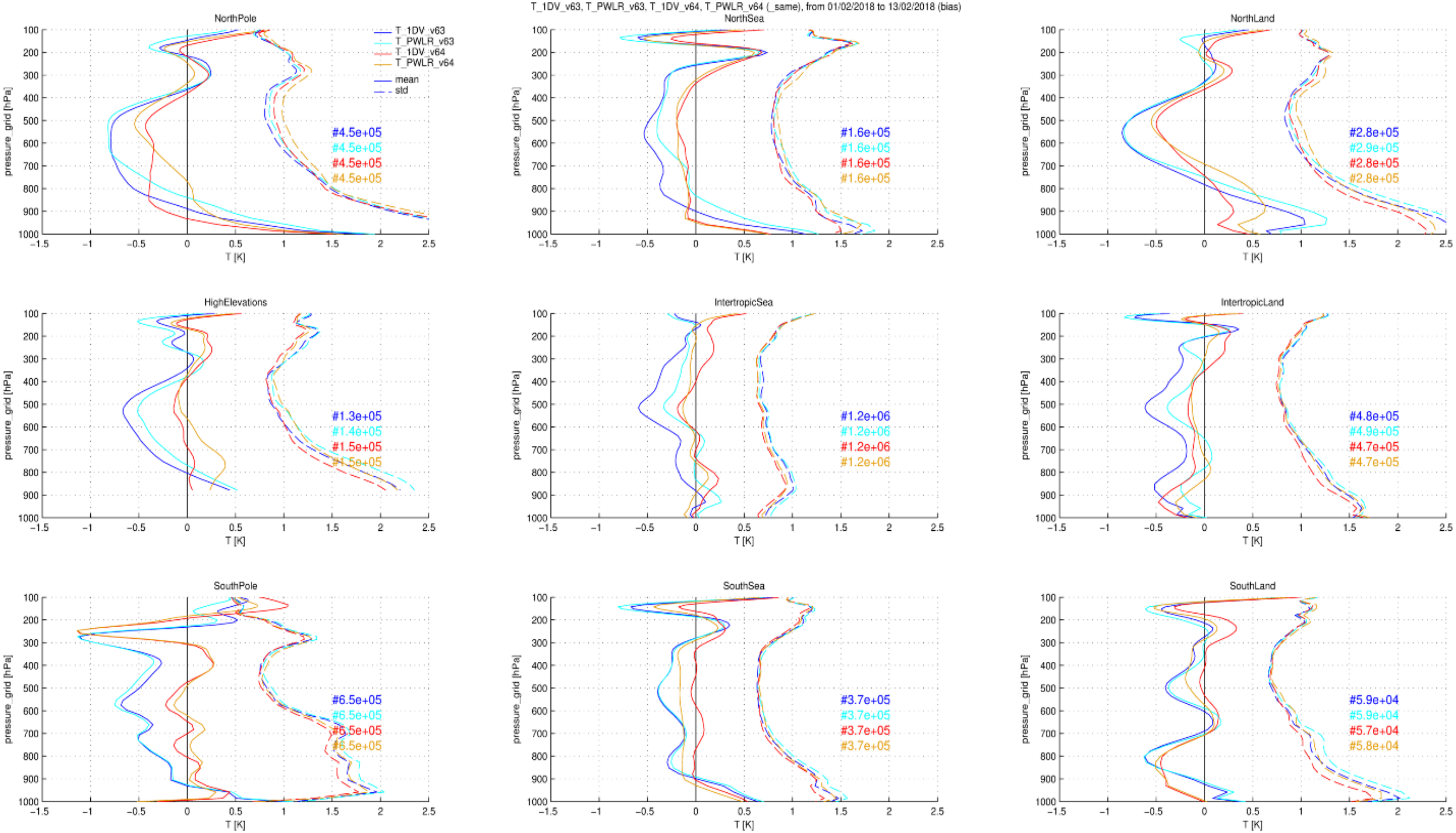

Figure 19: Comparison of temperature profiles from IASI L2 v6.3 (blue:OEM, cyan:PWLR³) and v6.4 (red: OEM, orange:PWLR³) to ECMWF analyses in regional classes, from Metop-B between 1 and 13 February 2018.

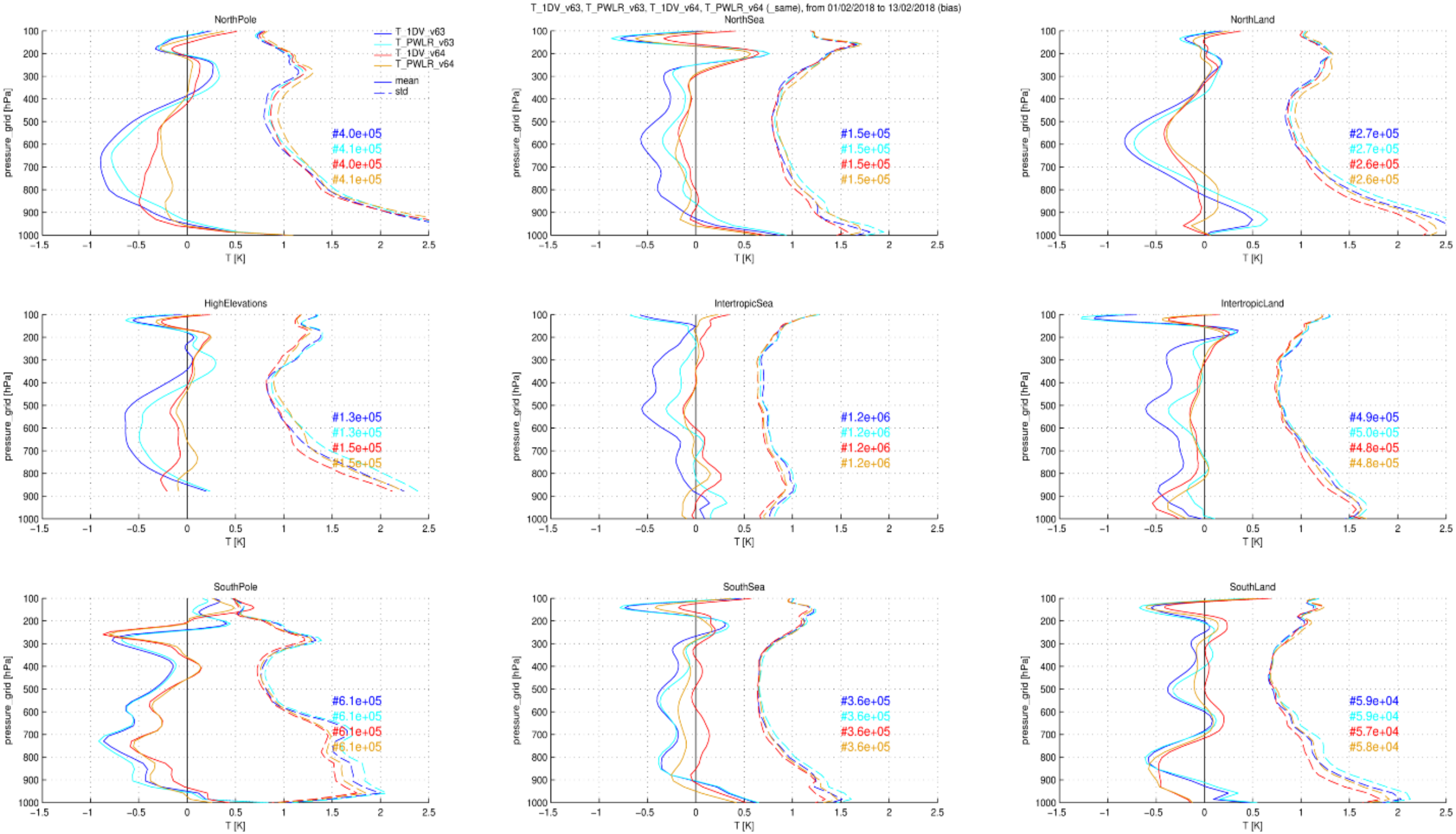

Figure 20: Comparison of temperature profiles from IASI L2 v6.3 (blue:OEM, cyan:PWLR³) and v6.4 (red: OEM, orange:PWLR³) to ECMWF analyses in regional classes, from Metop-A between 1 and 13 February 2018.

4.4 v6.3 and v6.4 humidity profiles vs ECMWF analysis

The water-vapour products from the operational (v6.3) and validation (v6.4) ground segments were compared to ECMWF analysis to allow global coverage and perform a stratification in land/sea and regional classes with statistically significant sample size, as explained in section 2.5. The statistics are summarised in the Figure 21 and Figure 22. The biases and standard deviations are improved in all classes with the OEM in v6.4 as compared to v6.3. This observation is consistently applicable to Metop-A and Metop-B products. The improvement is particularly noticeable over land, especially over Northern continental surfaces, with flatter and smaller biases by up to 0.2 g/kg and precision improved by 0.1 g/kg. This result is attributable to the improved first guess profiles, but also to the more accurate land surface emissivity retrieved in v6.4 with the PWLR[3] training on the CAMEL database with serves as input to the OEM retrieval of humidity. Overall, the OEM and PWLR[3] are of comparable precisions in v6.4, from 0.5 to 1 g/kg in the Northern hemisphere, to 1-1.5 g/kg in the equatorial band and in the Southern hemisphere in the period considered (1 to 13 February 2018).

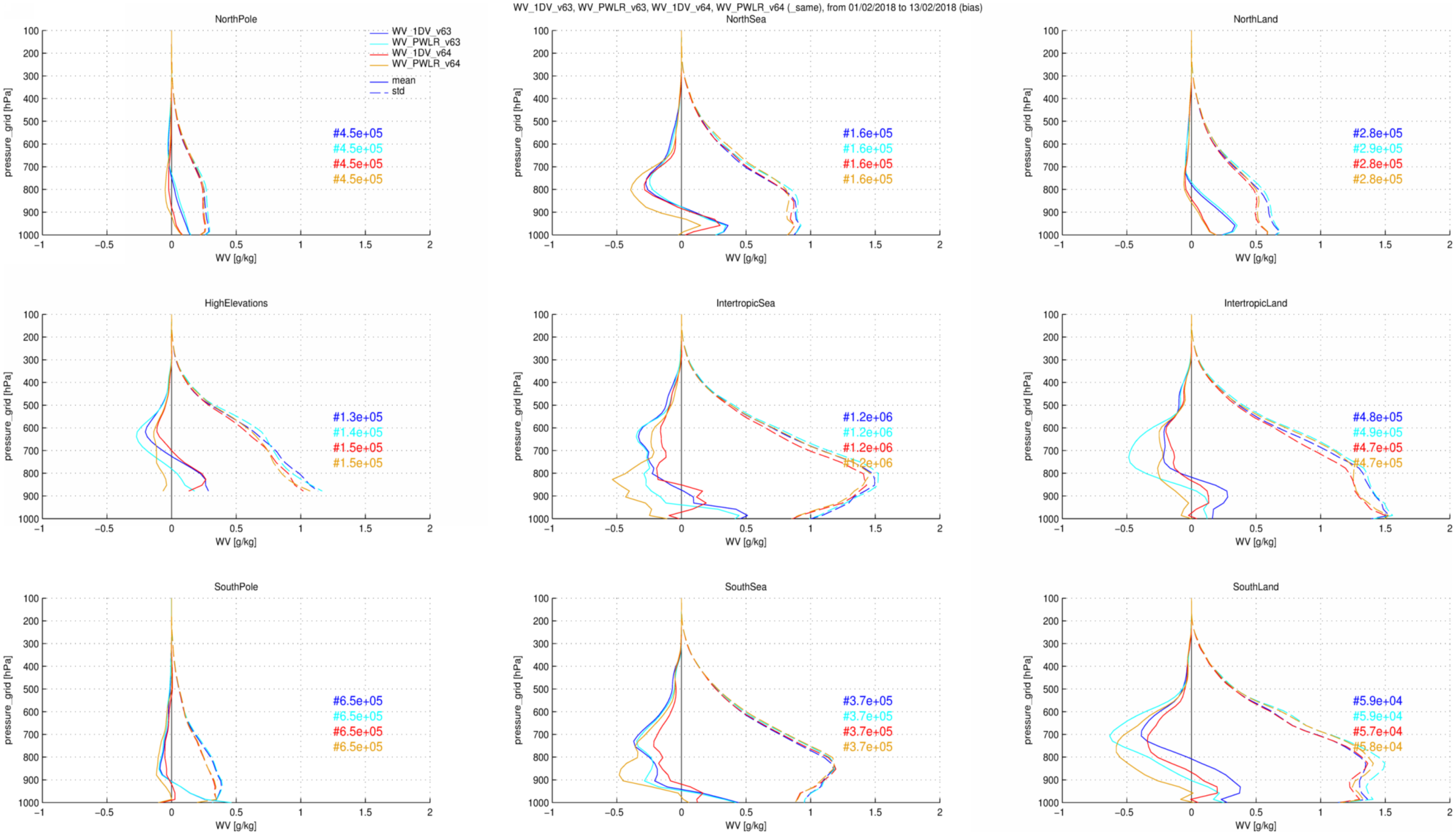

Figure 21: Comparison of humidity profiles from IASI L2 v6.3 (blue:OEM, cyan:PWLR³) and v6.4 (red: OEM, orange:PWLR³) to ECMWF analyses in regional classes, from Metop-B between 1 and 13 February 2018.

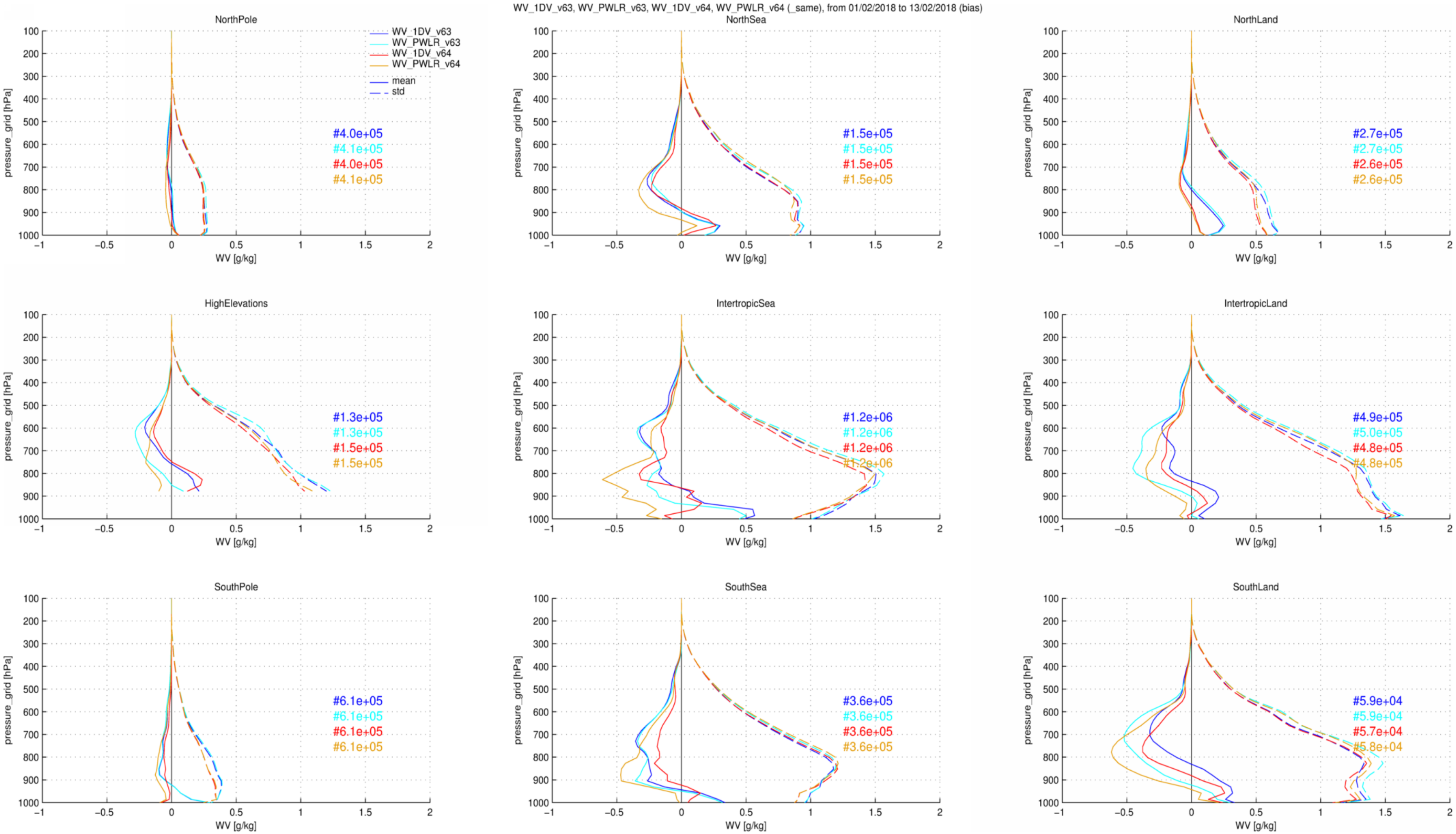

Figure 22: Comparison of humidity profiles from IASI L2 v6.3 (blue:OEM, cyan:PWLR³) and v6.4 (red: OEM, orange:PWLR³) to ECMWF analyses in regional classes, from Metop-A between 1 and 13 February 2018.

5 ASSESSMENT OF THE SEA SURFACE TEMPERATURE

The IASI L2 sea surface temperature (SST) product is routinely monitored with the Ocean and Sea-Ice Satellite Application Facility (OSI-SAF). As a conclusion of the product validation since the version 6, including comparison and monitoring with *in situ* drifting buoys, SST models and independent satellite products [RD-1, RD-7], the EUMETSAT IASI L2 SST has been included in the SST collection maintained by the Group for High Resolution SST (GHRSST) [RD-8]. EUMETSAT generates the L2Pcore products which are processed by the OSI SAF and formatted in the standard GHRSST L2P format.

As per SST L2P standard, the retrievals in every individual pixel are classified in Quality Levels (QL) from 5 (best quality) to 2 (low quality). The highest quality classes 3 to 5 are recommended for use as per GHRSST practices. A sensor specific error estimate (SSES) for each of the quality levels is included in the L2P SST products. The SSES are regularly reviewed and potentially subject to changes on a biannual basis when necessary, based on long-term monitoring against buoys.

The revision 6.4 of the IASI L2 operational processing chain updates slightly the quality control of the final SST retrieval (OEM) to perform the quality level assignment in the L2Pcore products. The SST retrieval itself also evolved in the v6.4 as a result of improving the first retrieval (PWLR[3]) and updating the RTTOV coefficients (see benefits on atmospheric products in section 3 and 4). We present here sample results of monitoring the SST from IASI L2 v6.3 (GS1, operational ground segment) and v6.4 (GS2, validation ground segment) against the OSTIA model (foundation SST) with the METIS monitoring facility [RD-9] and against ECMWF analyses, also based on OSTIA to analyse the sea skin surface temperature.

5.1 IASI v6.3 and v6.4 SST vs OSTIA

An anomaly was reported from the monitoring of IASI L2P SST against OSTIA with METIS facility [RD-9]. It is illustrated in the December time series (Figure 23), with a spike in the global standard deviation computed with IASI L2P SST on 18/12/2017, and with the daily maps from them monitoring (Figure 24). The problem originated in a cloud misclassification, when then cloud signal is small as can happen with low effective cloud amount or low/warm clouds. Such cases are however more correctly reflected in the quality indicator (error estimate) of the surface temperature (Ts) as generated with the first retrieval.

The quality control in the L2P SST has been therefore updated in v6.4 and now includes a check of the quality indicator for Ts from the PWLR[3], in addition to the stratification based on the cloud signal. The effect of the new quality control approach in v6.4 is illustrated in Figure 25, where another occurrence of these rare outliers is visible in the monitoring of the best three quality classes from v6.3 (red ellipses, top panel). They are correctly filtered out for a large majority in v6.4 (bottom panel).

An example of the statistics generated with the monitoring of the IASI L2P SST from the operational (v6.3) and validation (v6.4) ground segments is provided in Figure 26. The collocations of IASI and OSTIA and the distributions of their differences are computed on a daily basis for the three best quality classes (QL = 3, 4 or 5) together. The example shown is the 5 February 2018. The distributions obtained with v6.4 appear more Gaussian, with less of a cold tail than v6.3. The precision (standard deviation) is also better by 0.05 to 0.1 K globally from day to day with v6.4. The bias has changed as compared to OSTIA (which is the foundation SST), v6.4 appearing colder by 0.15 to 0.2 K on average for QL>3. Studies are on-going, using buoys from the long-term monitoring, to determine the new biases assigned in the SSES for each quality levels. In the interim period, also based on a more stratified comparison against ECMWF analysis (section 5.2), the biases in the SSES of the L2Pcore have been reset to 0. The standard deviations are left unchanged.

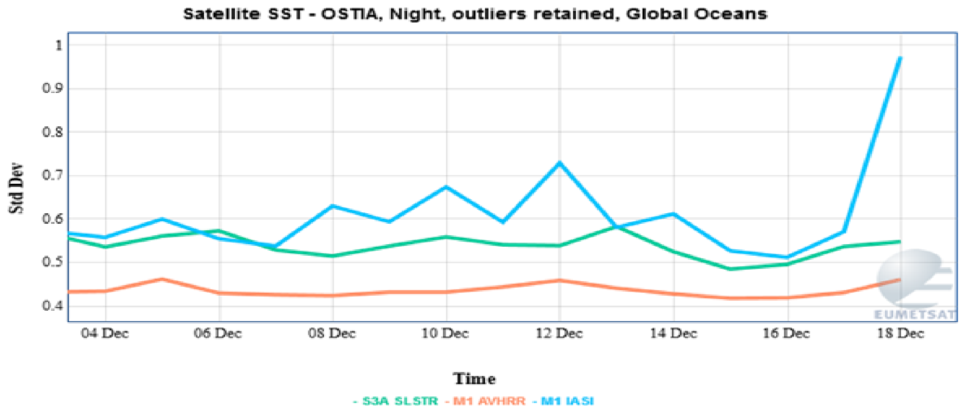

Figure 23: L2P SST monitoring in December 2017, IASI in cyan

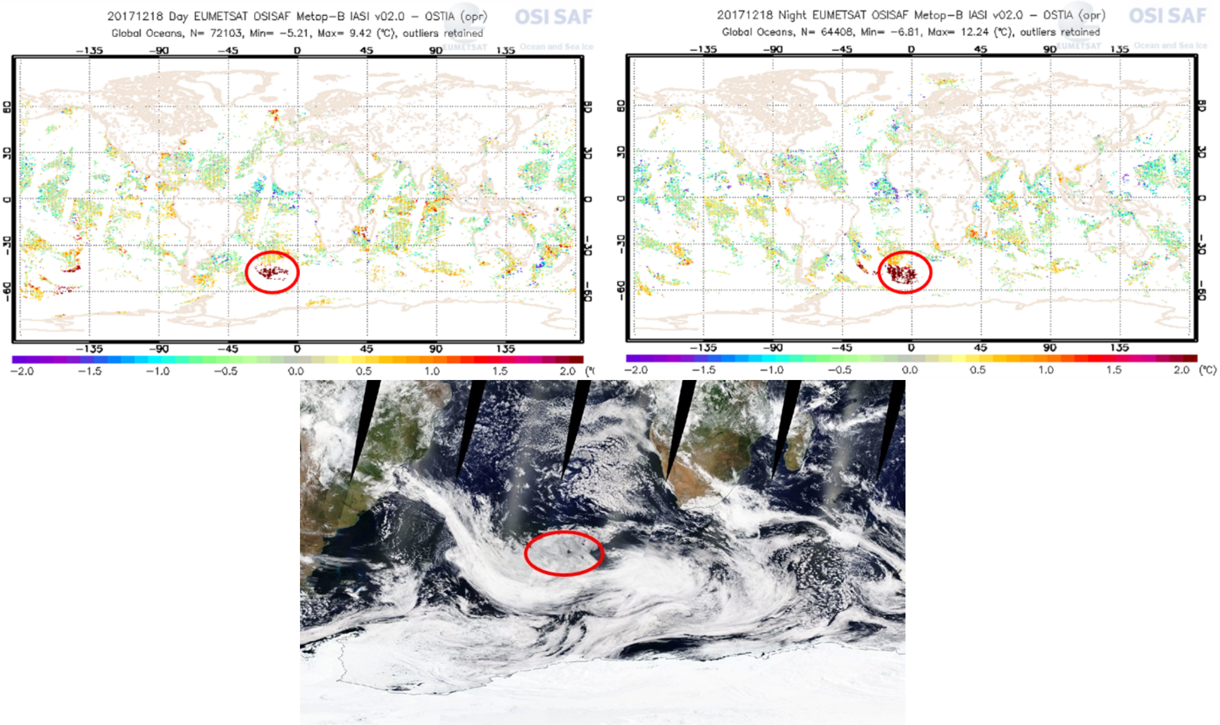

Figure 24: Anomaly in the IASI SST L2P product vs OSTIA (top left: day, top right: night) due to cloud misclassification (bottom MODIS RGB)

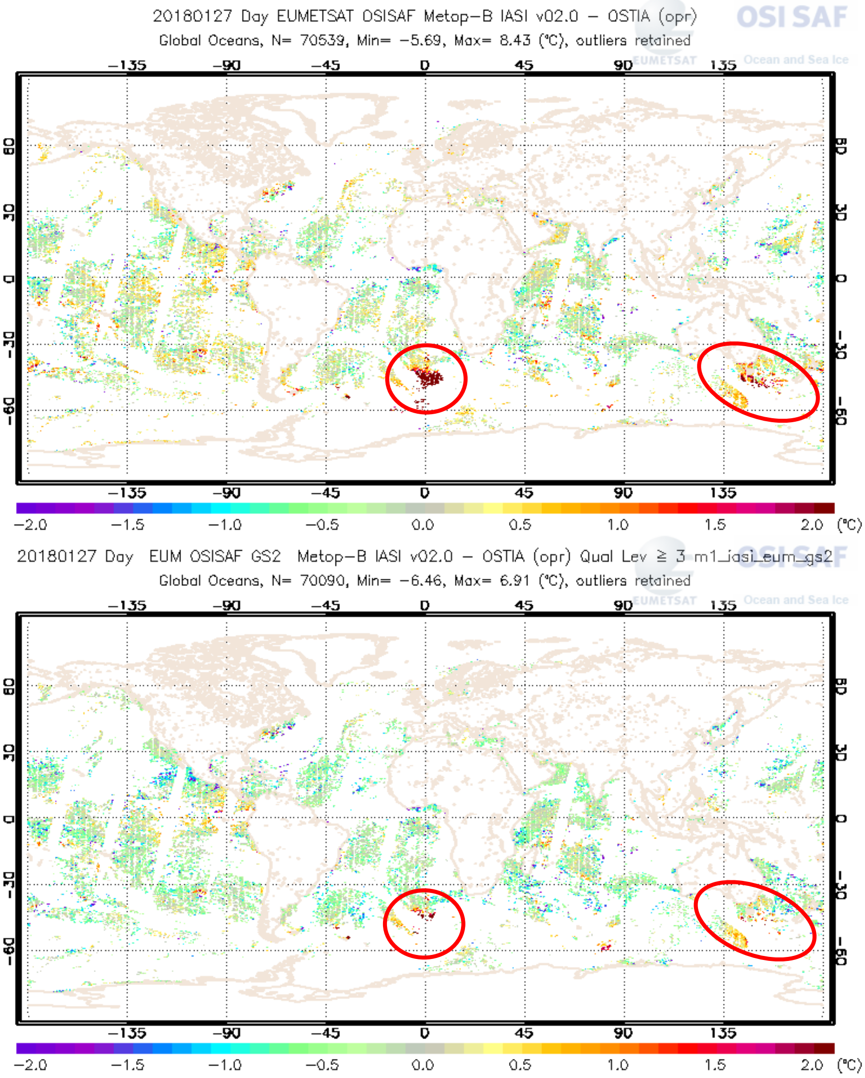

Figure 25: IASI vs OSTIA SST monitoring (QL 3 to 5) on 27 January 2018. The outliers in v6.3 (top, red ellipses) are filtered in v6.4 (bottom) as a result of updated quality control.

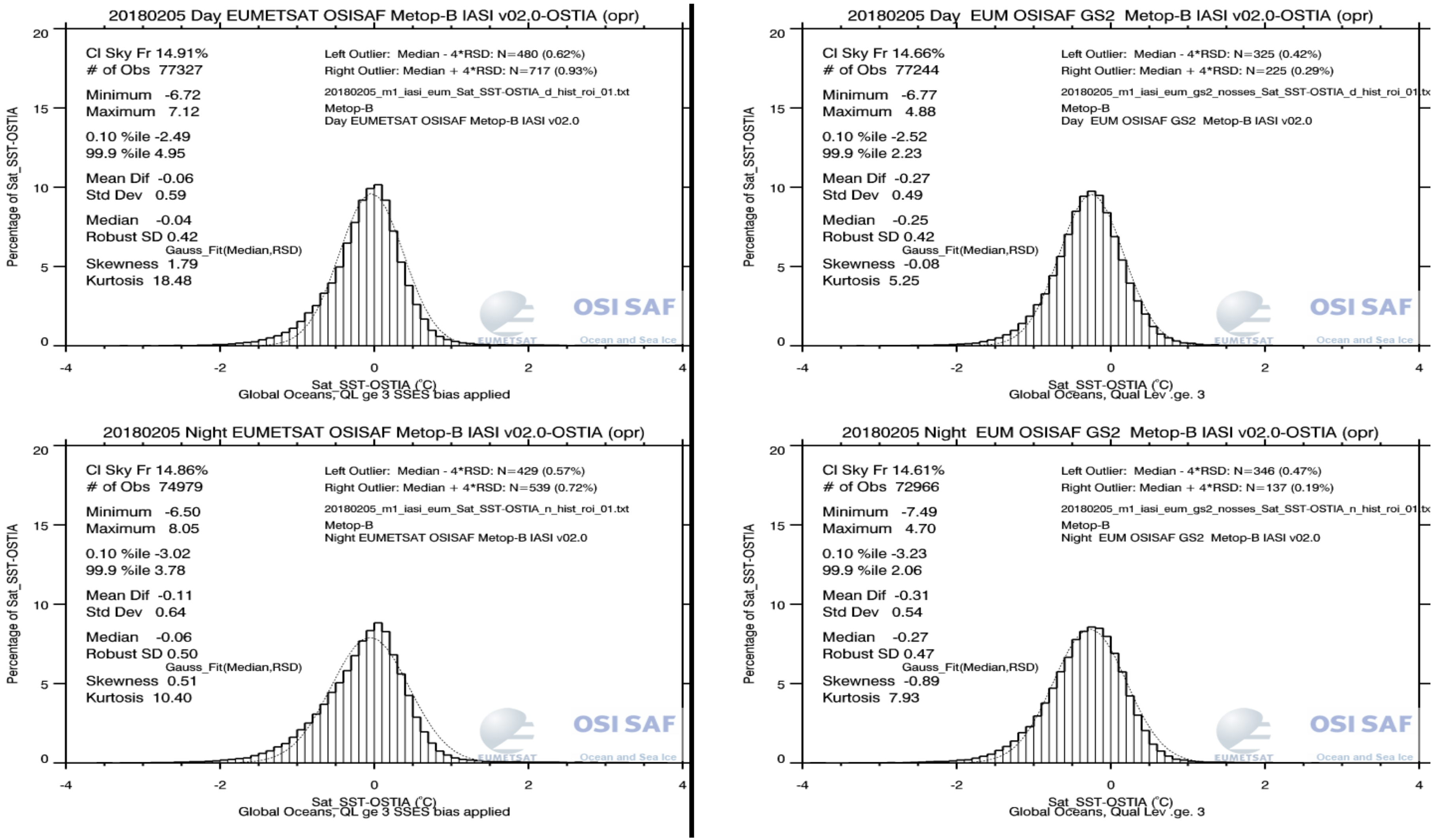

Figure 26: Routine daily monitoring of IASI L2P SST (left: operational v6.3 ; right: v6.4 in validation) vs OSTIA for day (top) and night (bottom) observations, on 05/02/2018.

5.2 IASI v6.3 and v6.4 SST vs ECMWF analysis

The routine monitoring of the operational products from GS1 with METIS is not yet stratified against the quality levels 3, 4 and 5 separately and does not yet include the QL2 (statistics are generated for all 3 best classes in combination). These features are only implemented for monitoring the validation ground segment (GS2) for now [RD-10]. Meanwhile, a more systematic assessment of the new quality classification approach and of the SST in each quality level was performed using ECMWF the skin SST analyses, which is a reactive parameter using the OSTIA foundation SST as input.

The statistics computed from two weeks of data with v6.3 (GS1, operational ground segment) and v6.4 (GS2, validation segment) between 1 and 13 February 2018 are presented in the figures Figure 27 to Figure 30. The mean difference, standard deviation and sample size from Metop-A and Metop-B are summarised in Table 2 (daytime) and Table 3 (nightime).

Overall, the standard deviations for Metop-A and Metop-B are similar in all quality classes with v6.4. Metop-B SST seem about 0.05 K colder than Metop-A in the first three quality classes. The bias in v6.4 (-0.02 to 0.13 K) is closer to 0 than with v6.3 (0.18 to 0.26 K) in the highest quality class (QL5). In the QL4, the bias is closer to 0 with v6.4 (-0.01 to -0.07 K) than with v6.3 (0.04 to 0.11 K) except for Metop-B at daytime (-0.12 vs 0.05). In the QL3 the bias has become colder by 0.1 to 0.15 K with Metop-B, it remains comparable to v6.3 for Metop-A. Overall the departures (IASI *minus* analyses SST) appear more Gaussian, symmetrical and with a better centred mode with v6.4 than with v6.3.

As compared to ECMWF SST, the precision (standard deviation) has improved with v6.4 by 0.05 K in the best quality class (QL5) while preserving the class sample size at night and even increasing the sample size by 5 to 7% at daytime. Likewise, the precision is improved with v6.4 by 0.1 to 0.2 K in the quality classes 4 and 3. The sample size in QL4 with v6.3 and v6.4 are comparable. We note the sample size in QL3 has decreased with v6.4 (with improved precision) while the number of retrievals classified in QL2 (low quality – not for use) has slightly increased in v6.4. This overall confirms the benefits of the updated quality control strategy introduced in v6.4. Noteworthy, the number of low quality SST remains small, relatively to the three best quality samples (QL2 forms approximately 7% of the total number of SST retrievals).

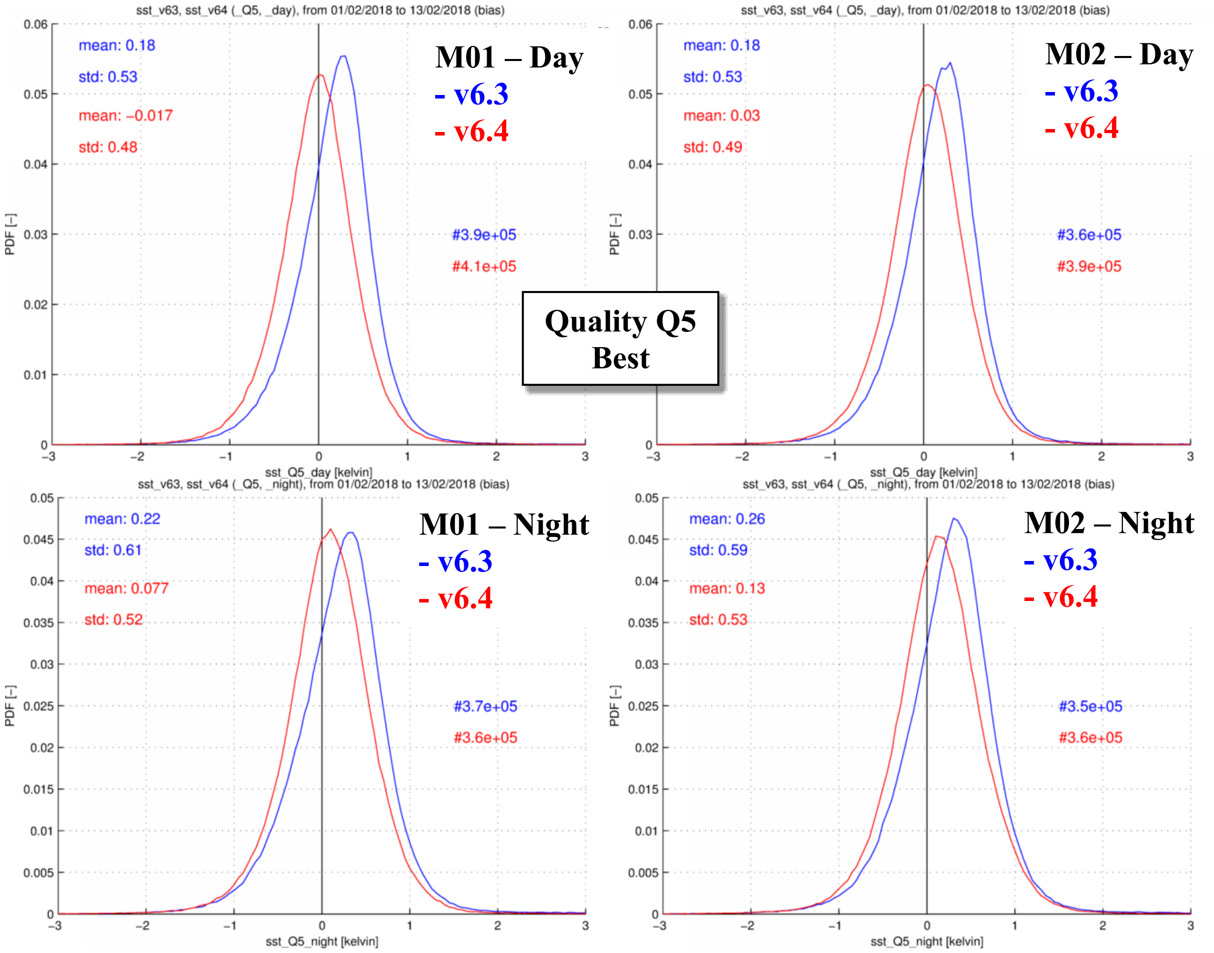

Figure 27: Quality class 5 (best) IASI L2P SST v6.3 (blue) and v6.4 (red) vs ECMWF skin SST analyses between 1 and 13 February 2018. Metop-B (left) and Metop-A (right) at day (top) and night (bottom).

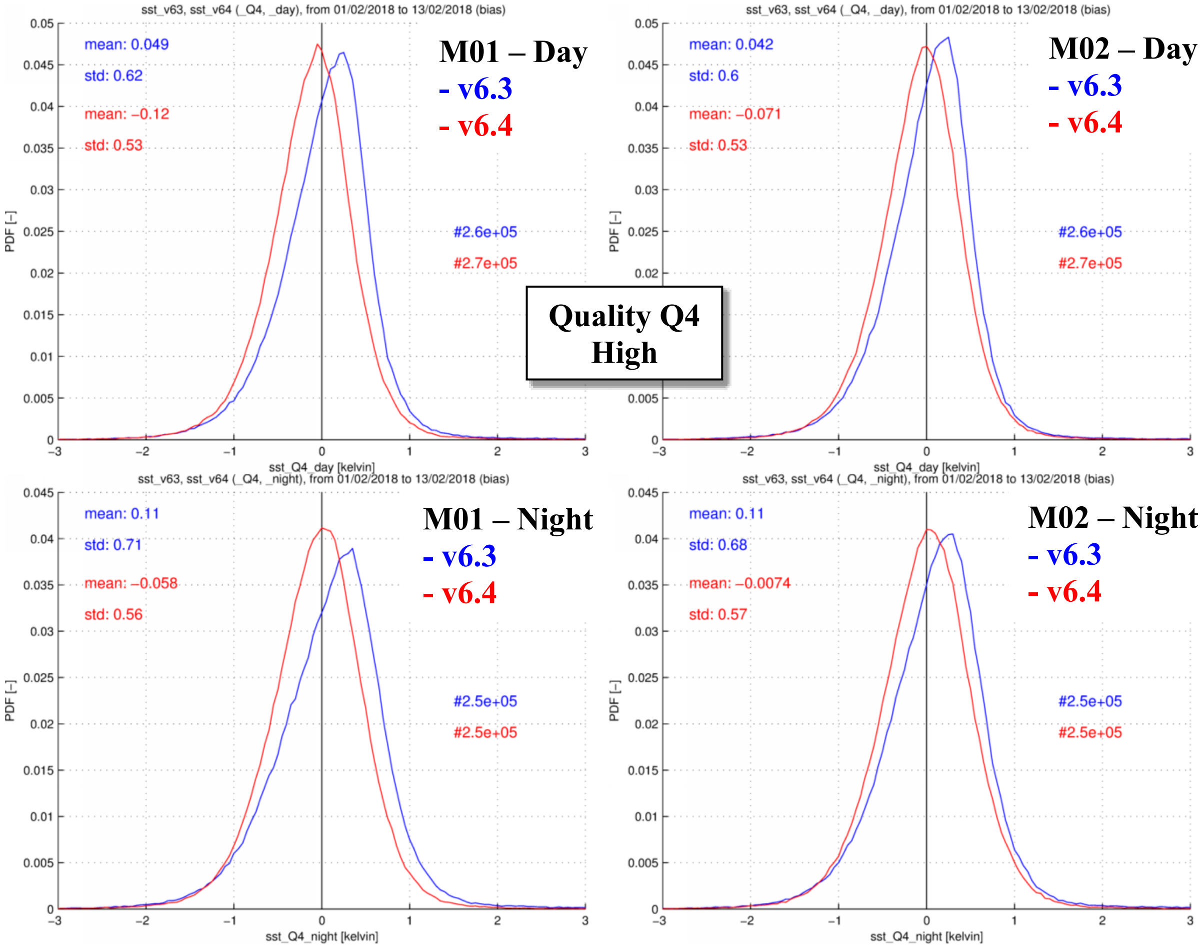

Figure 28: Quality class 4 (high) IASI L2P SST v6.3 (blue) and v6.4 (red) vs ECMWF skin SST analyses between 1 and 13 February 2018. Metop-B (left) and Metop-A (right) at day (top) and night (bottom).

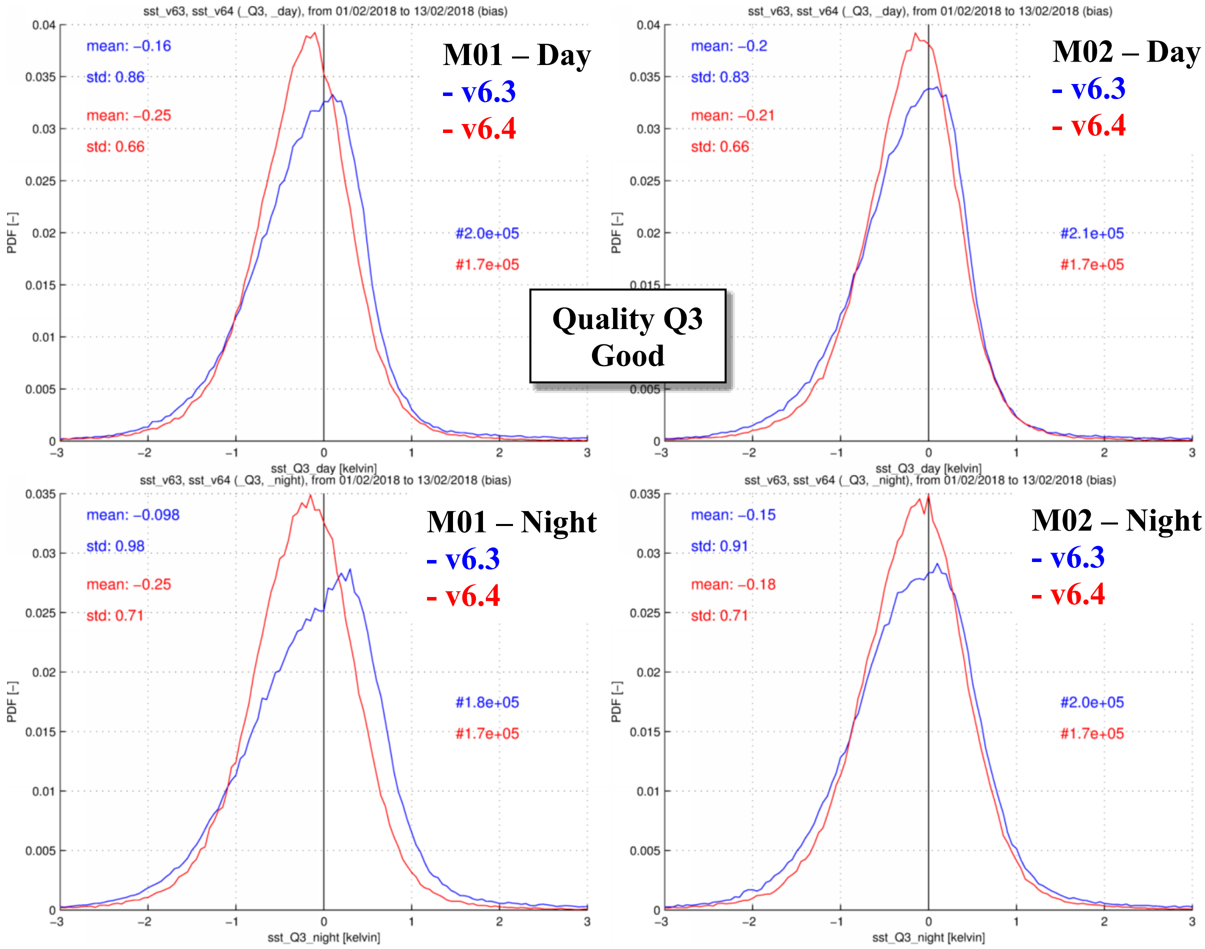

Figure 29: Quality class 3 (good) IASI L2P SST v6.3 (blue) and v6.4 (red) vs ECMWF skin SST analyses between 1 and 13 February 2018. Metop-B (left) and Metop-A (right) at day (top) and night (bottom).

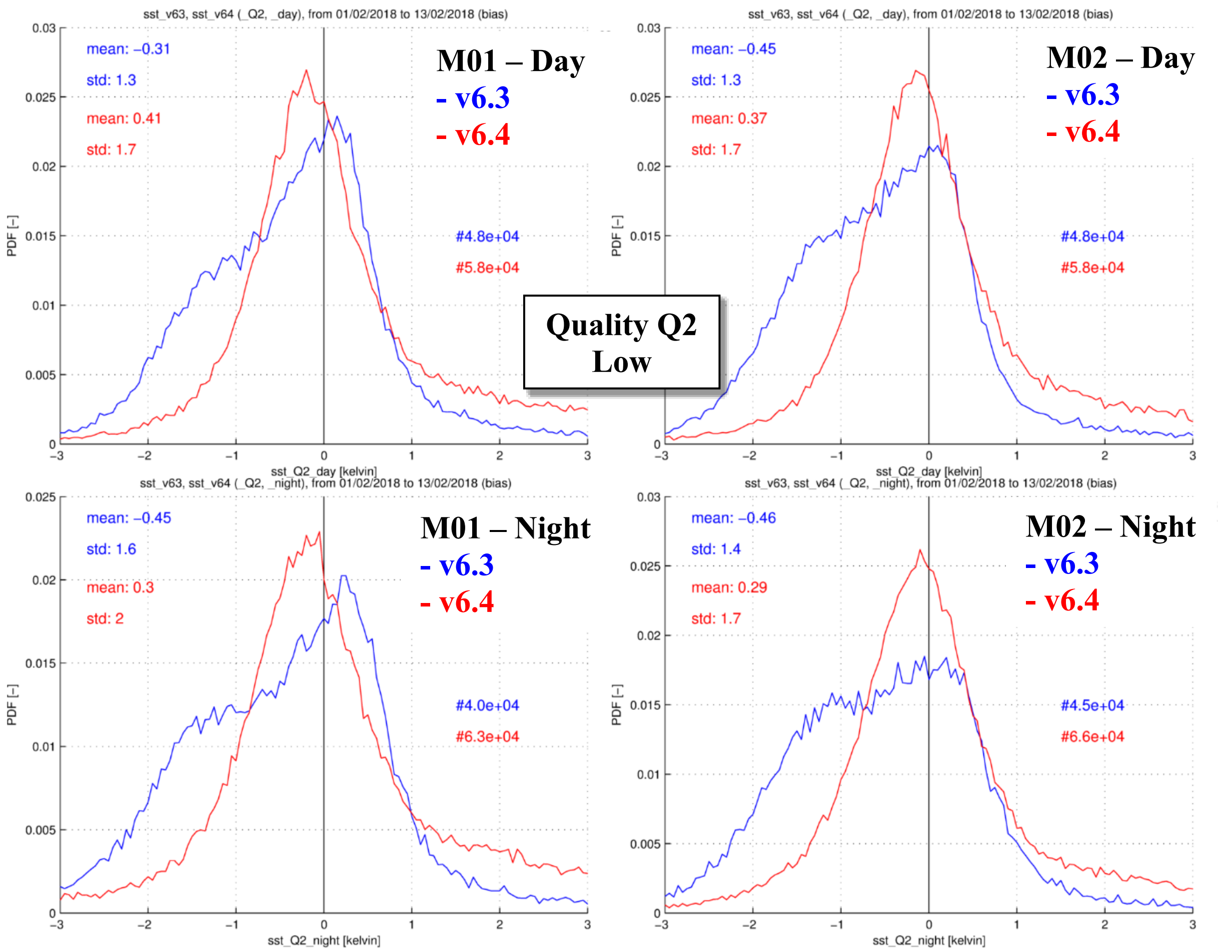

Figure 30: Quality class 2 (low – not for use) IASI L2P SST v6.3 (blue) and v6.4 (red) vs ECMWF skin SST analyses between 1 and 13 February 2018. Metop-B (left) and Metop-A (right) at day (top) and night (bottom).

	Day											
	Metop-A						Metop-B					
	V6.3			V6.4			V6.3			V6.4		
	Bias (K)	σ (K)	# ($x10^4$)	bias (K)	σ (K)	# ($x10^4$)	bias (K)	σ (K)	# ($x10^4$)	bias (K)	σ (K)	# ($x10^4$)
QL5	0.18	0.53	36	0.03	0.49	39	0.18	0.53	39	-0.02	0.48	41
QL4	0.04	0.6	26	-0.07	0.53	27	0.05	0.62	26	-0.12	0.53	27
QL3	-0.2	0.83	21	-0.21	0.66	17	-0.16	0.86	20	-0.25	0.66	17
QL2	-0.45	1.3	4.8	0.37	1.7	5.8	-0.31	1.3	4.8	0.41	1.7	5.8

Table 2: Summary of the differences IASI L2Pcore SST – ECMWF analyses in each quality classes. Daytime products between 1 and 13 February 2018

	Night											
	Metop-A						Metop-B					
	V6.3			V6.4			V6.3			V6.4		
	Bias (K)	σ (K)	# ($x10^4$)	bias (K)	σ (K)	# ($x10^4$)	bias (K)	σ (K)	# ($x10^4$)	bias (K)	σ (K)	# ($x10^4$)
QL5	0.26	0.59	35	0.13	0.53	36	0.22	0.61	37	0.08	0.52	36
QL4	0.11	0.68	25	-0.01	0.57	25	0.11	0.71	25	-0.06	0.56	25
QL3	-0.15	0.91	20	-0.18	0.71	17	-0.1	0.98	18	-0.25	0.71	17
QL2	-0.46	1.4	4.5	0.29	1.7	6.6	-0.45	1.6	4.0	0.3	2.0	6.3

Table 3: Summary of the differences IASI L2Pcore SST – ECMWF analyses in each quality classes. Night-time products between 1 and 13 February 2018

5.3 Comparisons against buoy SST with the OSI SAF matchup dataset

When the new version has been implemented operationally, the OSI SAF will produce routinely the OSI SAF IASI matchup dataset of satellite observations collocated with drifting buoys for the new version. This will be further analysed at EUMETSAT to update the SSES assigned to the different quality classes. In the meantime, for the activation of IASI L2 v6.4 products, the biases have been reset to 0 K and the standard deviations left unchanged from v6.3.

6 ASSESSMENT IN RADIANCE SPACE OF THE PARAMETERS RETRIEVED WITH THE FIRST RETRIEVAL ($PWLR^3$)

In this section, the products from the first retrieval ($PWLR^3$) are analysed in the radiance space, by assessing how well the IASI observations (OBS) can be fitted with calculated (CALC) radiances, using the retrieved parameters as input to RTTOV as a forward model. The $PWLR^3$ is a statistical algorithm which does not minimise the OBS-CALC residuals, unlike the optimal estimate. It is therefore expected that these residuals are more directly linked to the precision of the retrieved profiles. We present hereafter intercomparisons of OBS-CALC differences computed in turn with the $PWLR^3$ retrievals in v6.4, v6.3, static atlas and with numerical model data. The statistics are analysed in the IASI band 1 and band 2, to avoid potential confusion from modelling the solar radiations in the band 3.

6.1 Focus on land surface emissivity

Land surface emissivity is a difficult product to validate, as there does not exist independent fiducial reference like this there is for SST (e.g. drifting buoys), atmospheric temperature and humidity (e.g. sondes)… The relative merits of different land surface emissivity datasets can be indirectly assessed through inspections of the OBS-CALC residuals, which were computed here for continental cloud-free cases with reprocessed Metop-B observations on 01/11/2017. The quality control to retain cloud-free pixels was based on the OmC parameters (|OmC]<1.5 K) and the quality indicator for surface temperature (<2 K) retrieved with the $PWLR^3$.

The Figure 32 shows the improvements in OBS-CALC with retrieved land surface emissivity (black, $PWLR^3$ from v6.4) as compared to using the latest to date emissivity atlas CAMEL atlas, from University of Wisconsin [RD-15]. Noteworthy, the $PWLR^3$ v6.4 was actually trained with the CAMEL atlas. These results illustrate how a statistical retrieval can be more precise (reduced random error) than its training base. The associated land cases are located at mid and lower latitudes (|lat| < 60°), as illustrated in the Figure 31. The improvements from using the retrievals over the static atlas are higher in the window region between 1100 and 1200 cm^{-1}, where the natural variance of the land surface emissivity is also higher than in the 800-1000 cm^{-1} window region [RD-21]. Despite the natural variance of emissivity being small in the 800-1000 cm^{-1} window region, small improvements to the radiance fit are still observed with the $PWLR^3$ retrievals.

The same intercomparison was repeated for continental Polar pixels (|lat|>60°) and are shown in Figure 33. In this case, the gain in fitting the observations with the retrieved emissivity is as important in both window regions, showing the benefits of using the statistical land emissivity retrievals for snow/ice cover as well, compared to a static atlas.

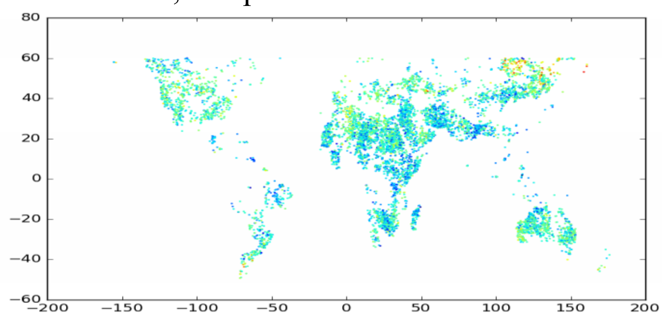

Figure 31: Location of pixels used in Figure 32, 01/11/2017

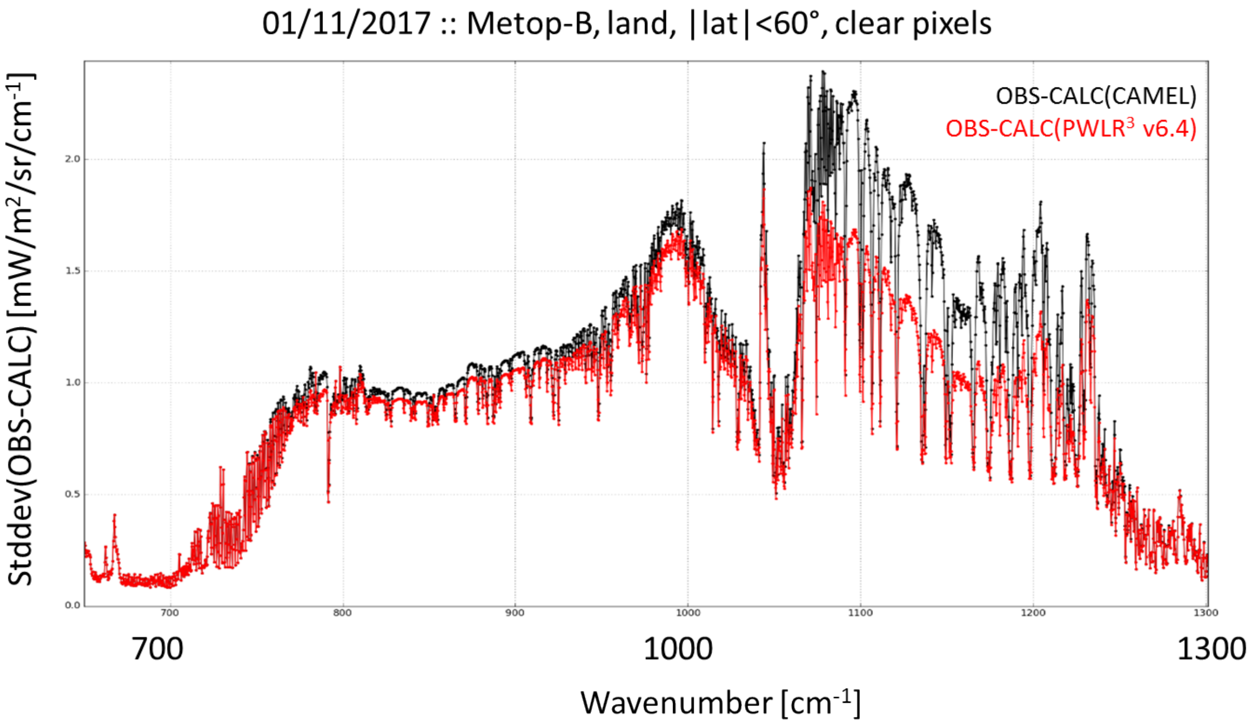

Figure 32: Continental OBS-CALC with different land surface emissivity dataset: PWLR³ LSE (red) and CAMEL static (black). Metop-B, mid- and low-lat on 01/11/2017

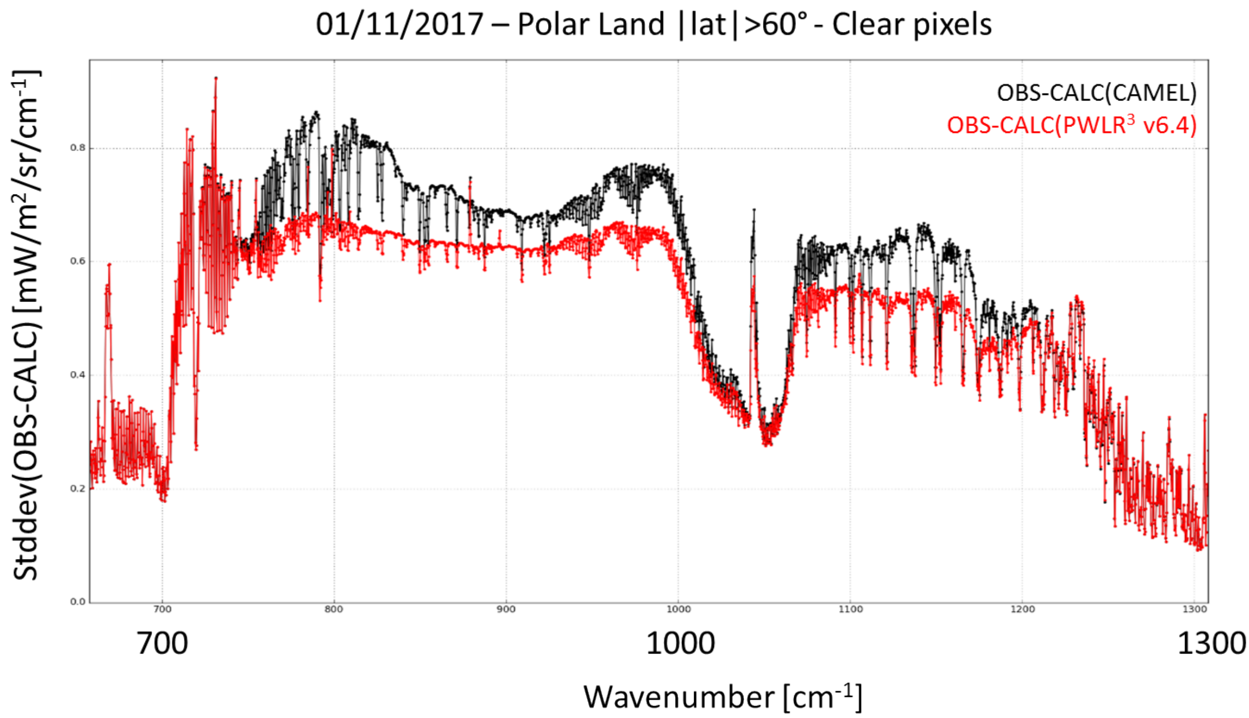

Figure 33: Same as Figure 32, in the Polar caps, with |lat|>60°.

The OBS-CALC was computed for the same non-Polar sample as in Figure 32, using ECMWF forecasts for the temperature, humidity and ozone, together with the static emissivity atlas. The results are shown in the Figure 34, which illustrates the advantages of both the land and atmospheric parameters as retrieved with the PWLR³ v6.4 over land to reproduce the IASI observations.

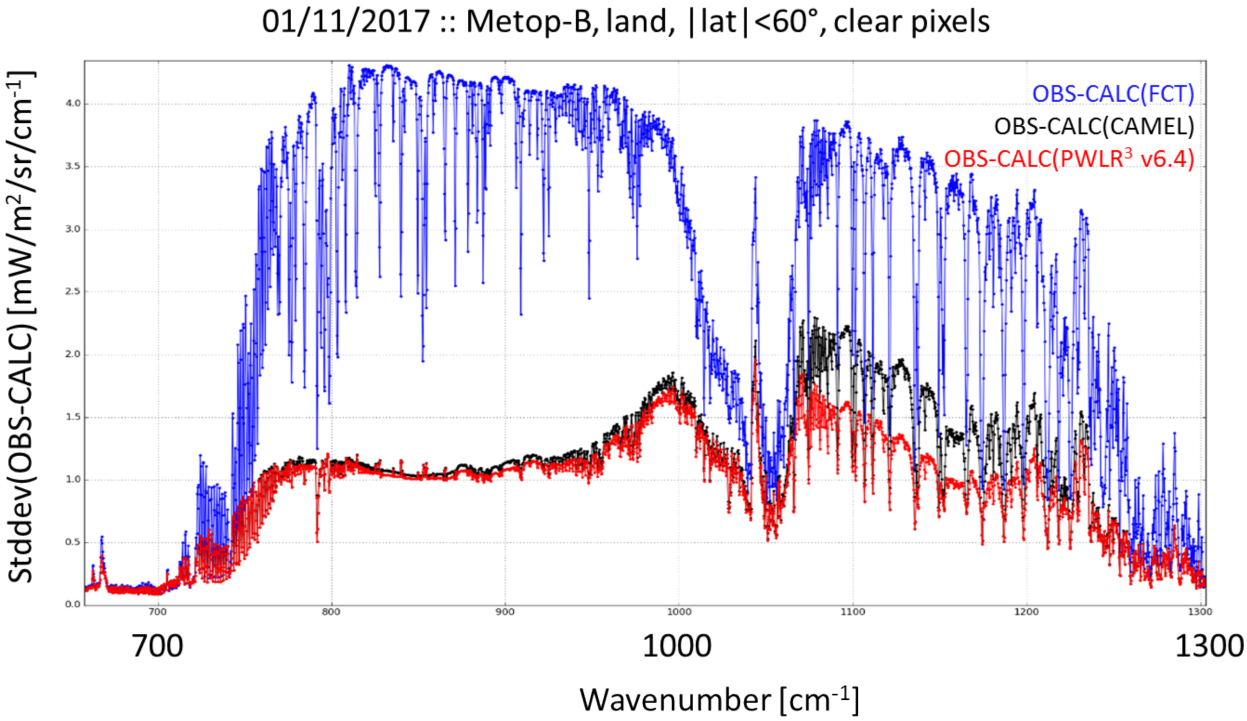

Figure 34: Same as Figure 32 with the addition (in blue) of CALC computed with ECMWF forecasts + static emissivity atlas.

6.2 Zoom in the ozone region

In the following, different OBS-CALC were computed with different sources of information for ozone, in maritime cloud-free situations with reprocessed Metop-B observations on 01/12/2016. The other geophysical parameters used as input to RTTOV radiance simulations (temperature and humidity profiles and surface temperature) are from the $PWLR^3$ v6.4 retrievals. The sea surface emissivity is computed after the RTTOV built-in infrared sea surface emissivity model. The Figure 35 shows the standard deviation of the residuals computed in the main ozone spectral region of IASI, with ozone profiles from CAMS (purple), ECMWF forecasts (blue), ERA-5 (red) and $PWLR^3$ retrieval (black). It can be seen that among the different numerical models, the ozone from ERA-5 yields the best fit to the observations. The IASI observations are in the end best fitted with the $PWLR^3$ ozone retrieval, which was trained with ERA-5 data. This shows in the context of ozone as well how statistical methods can yield better precision (lower random error) than their underlying training base.

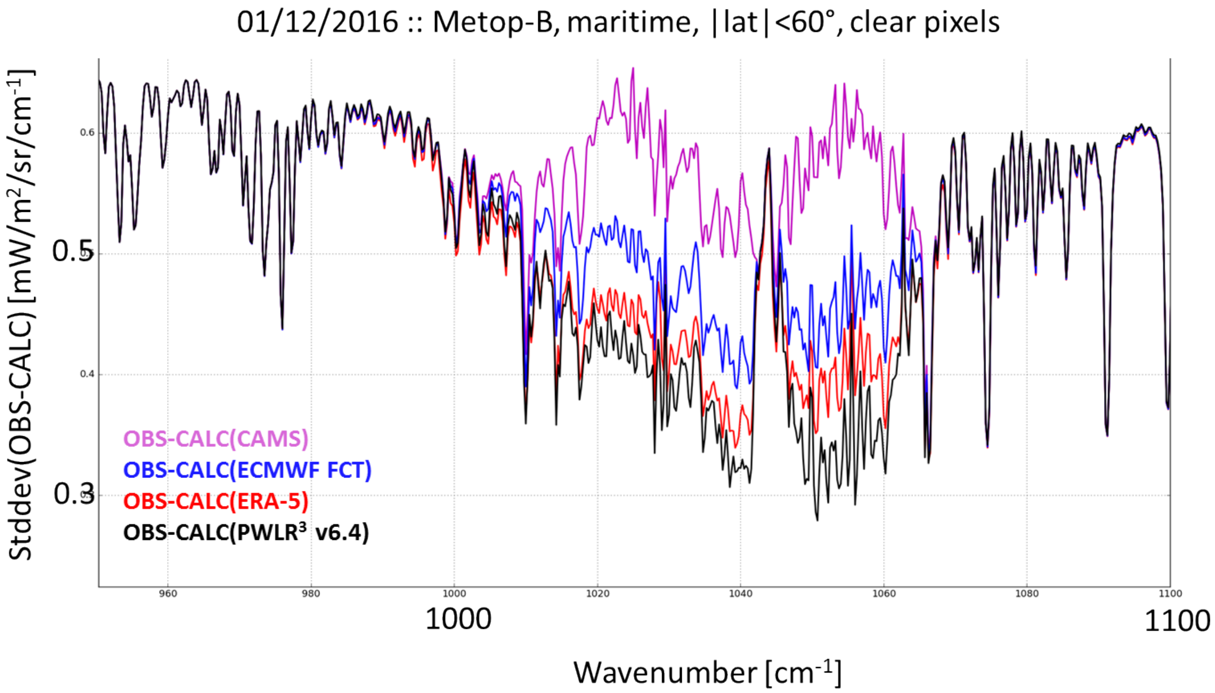

Figure 35: Maritime OBS-CALC with different ozone datasets: CAMS (purple), ECMWF FCT (blue), ERA-5 (red), PWLR³ (black). Metop-B, mid- and low-lat on 01/12/2016

6.3 Residuals from v6.3 (GS1), v6.4 (GS2) and NWP forecasts in IASI bands 1 and 2

In the following, we compare OBS-CALC using PWLR³ retrievals with v6.3 (from the operational ground segment GS1), with v6.4 (from the validation ground segment GS2) and with ECMWF forecast fields. The statistics have been computed with Metop-B data from 1 to 3 February 2018, in cloud-free pixels according to FLG_CLDNES.

The statistics are presented for maritime and continental cases separately in the section 6.3.1 and 6.3.2, respectively. In both stratifications, we retained low- and mid-latitudes sensing, with latitude within [60°S ; 60°N].

6.3.1 Maritime scenes

The Figure 36 displays the standard deviation of the OBS-CALC computed over oceans at mid and low latitudes with the sea surface temperature and temperature, humidity and ozone profiles respectively coming from IASI L2 v6.3 (red), v6.4 (black) and ECMWF forecast (blue). The quality control for pixel selection includes cloud-free pixels (as per FLG_CLDNES) with successful optimal estimation retrievals, quality indicator for temperature PWLR³ QT < 2 K and quality indicator for surface temperature QTs < 0.55 K. v6.4 yields best fit in nearly all spectral regions, except around OBS-CALC using forecasts are slightly lower or comparable to v6.4. v6.4 is an improvement in the entire spectral domain as compared to residuals from v6.3.

Both PWLR³ v6.3 and v6.4 retrievals yield lower random OBS-CALC errors than ECMWF forecasts in the CO_2/temperature and in the water-vapour spectral regions. To disambiguate the contributions from the surface and from the atmospheric profiles in the ability to fit the observations, the same SST (from the OEM v6.4) was assigned to all three OBS-CALC computations. The results are presented in the Figure 37, where it is confirmed that the retrieved profiles allow better OBS-CALC than the forecasts in the entire IASI bands 1 and 2. The PWLR^3 v6.4 yield the best fit, improving slightly over v6.3, in all channels.

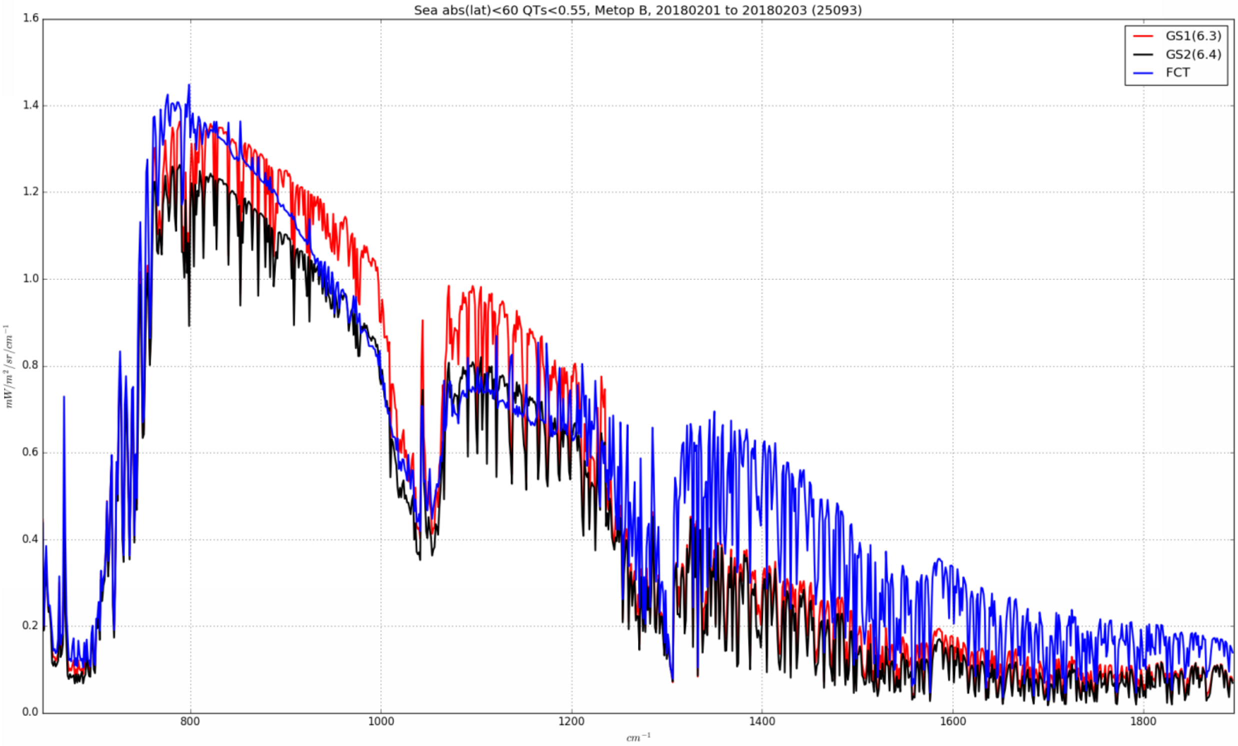

Figure 36: Maritime OBS-CALC computed with PWLR^3 v6.3 (from GS1, red), PWLR^3 v6.4 (from GS2, black) and with ECMWF forecasts (blue). Metop-B cloud-free pixels from 1 to 3 February 2018

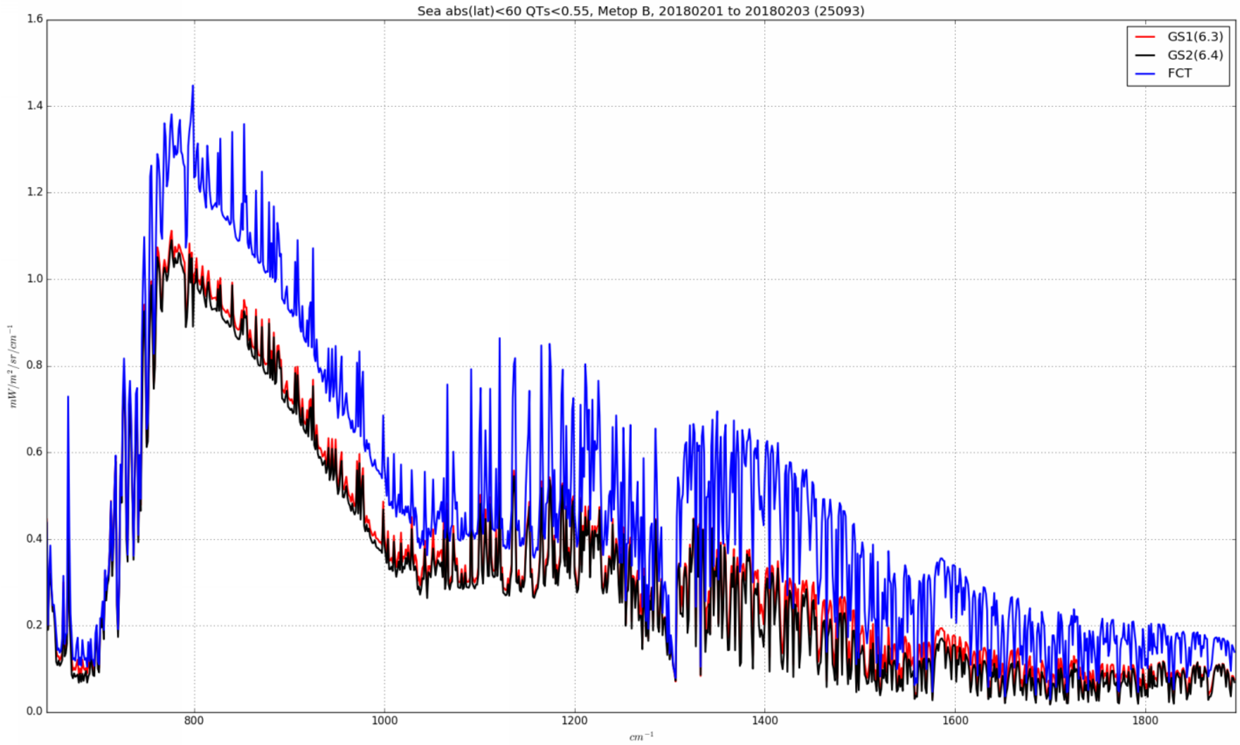

Figure 37: Same as Figure 36, with the same SST (from OEM v6.4) for all 3 OBS-CALC

6.3.2 Continental scenes

The Figure 38 and Figure 39 display the standard deviation of the OBS-CALC computed over land for latitudes within [60°S ; 60°N], using the surface temperature and temperature, humidity and ozone profiles respectively coming from IASI L2 v6.3 (red), v6.4 (black) and ECMWF forecast (blue). The surface emissivity used with the forecasts comes from the static CAMEL atlas [RD-15], while it is the land surface emissivity as respectively retrieved in the v6.3 and v6.4 statistics. The quality control for pixel selection includes cloud-free pixels (as per FLG_CLDNES) with successful optimal estimation retrievals, quality indicator for temperature PWLR^3 QT < 2 K. The PWLR^3 v6.3 and v6.4 retrievals yield better fit than the forecast fields in all spectral regions, with v6.4 fitting best the IASI observations in nearly all channels, confirming the overall improvements with this new release.

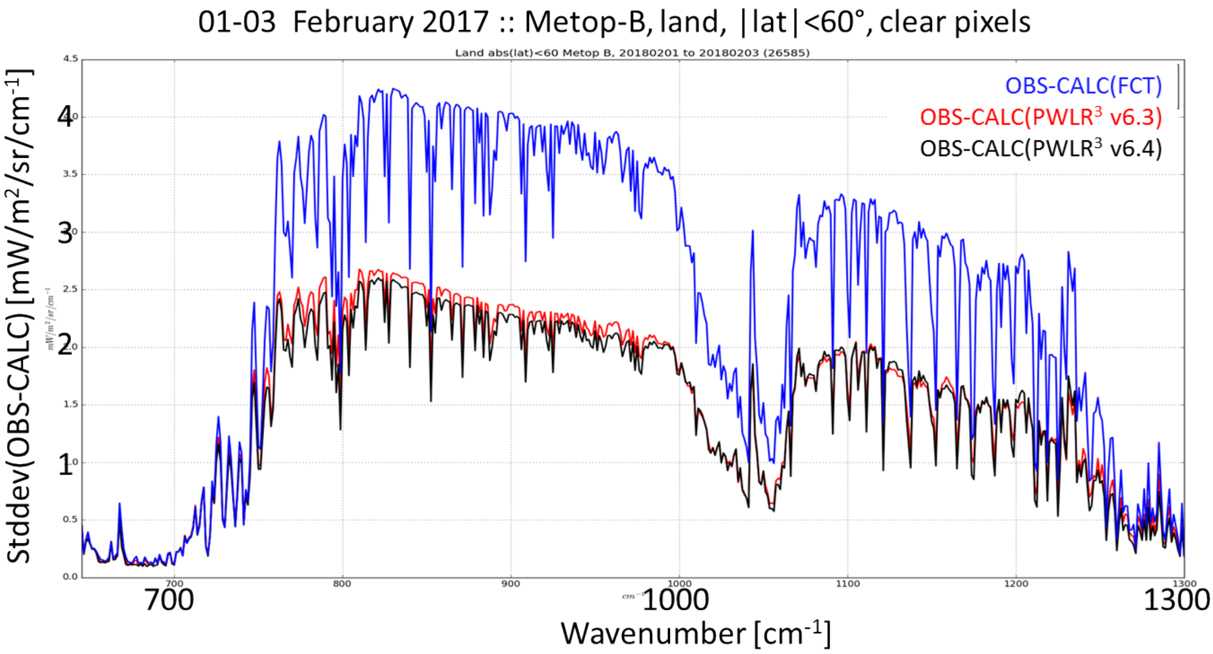

Figure 38: Continental OBS-CALC computed in IASI band 1 with PWLR^3 v6.3 (from GS1, red), PWLR^3 v6.4 (from GS2, black) and with ECMWF forecasts (blue). Metop-B cloud-free pixels from 1 to 3 February 2018

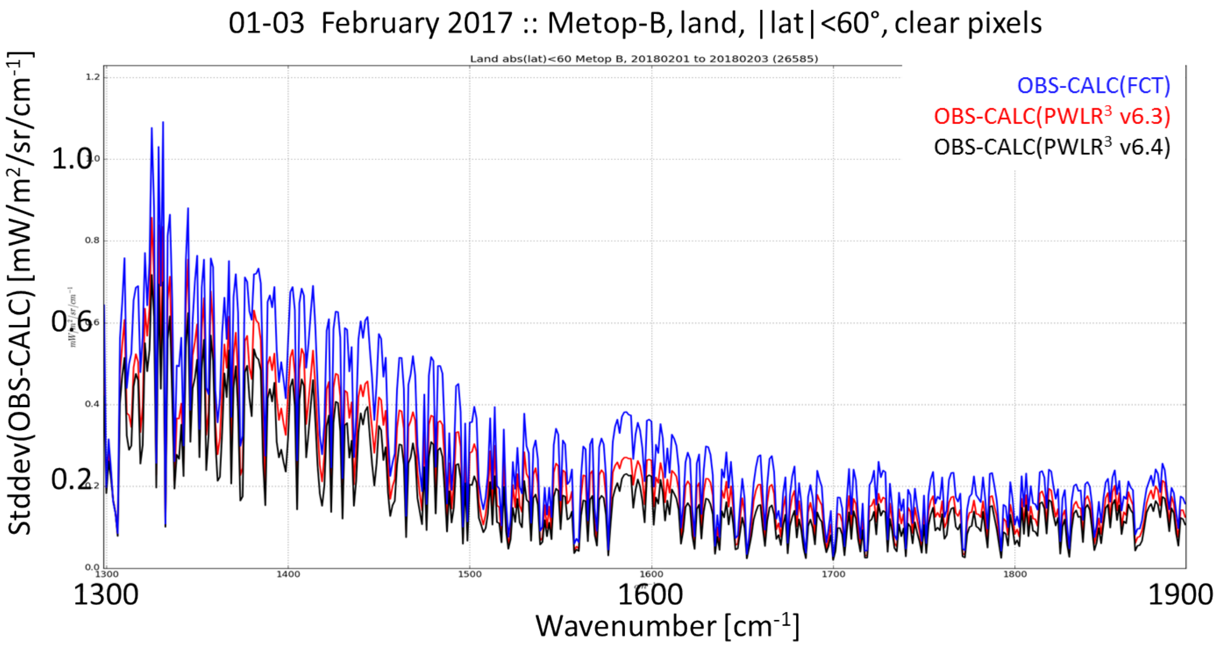

Figure 39: Same as Figure 38, in IASI band 2 (water-vapour region)

7 VERIFICATION OF REGIONAL AND GLOBAL PROCESSING

The EARS-IASI Level 2 regional service builds on the EARS-IASI system and implements for regional processing the fast statistical retrieval method PWLR[3], which forms the first retrieval step of the global IASI L2 processor. The products are available to the users within 30 minutes from sensing [RD-20]. The geographical coverage is shown in Figure 41.

The Figure 40 shows the elements of the IASI L2 processor (high-level overview in Figure 1) retained in EARS-IASI L2. The regional service has been running in a Demonstrational mode since November 2016 and entered a Pilot phase in November 2017.

The objective of the work presented in this section is to verify that the regional and global products are consistent, to a level that makes validation results obtained with the global products (and presented in the previous sections) directly applicable to the regional products (EARS-IASI L2). The data used were generated from the respective validation ground segment of the global and regional processing with data from 16 February 2018.

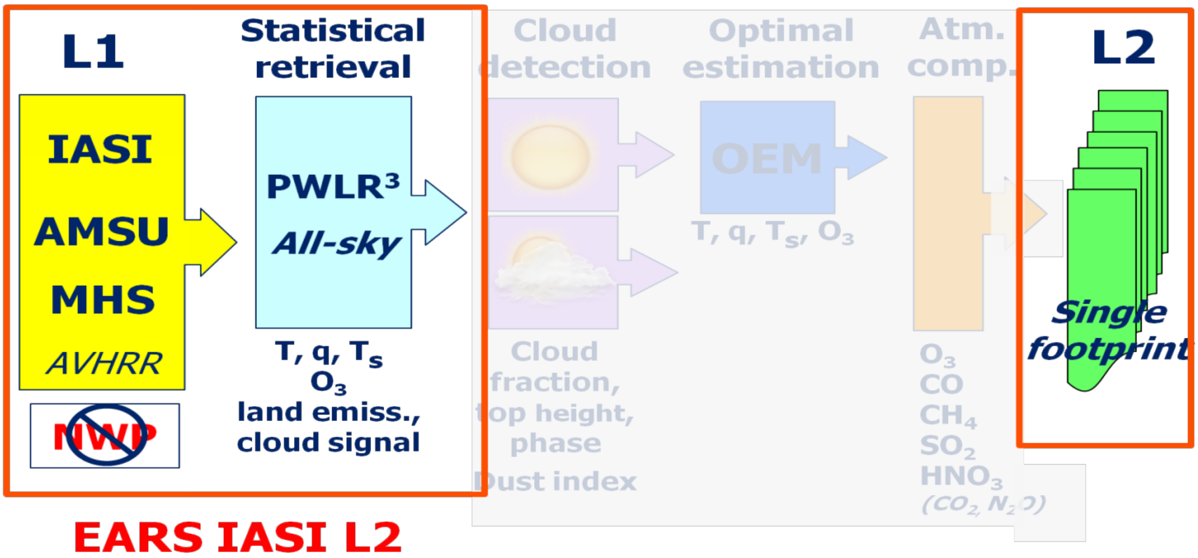

Figure 40: High level overview of the IASI L2 functions retained for regional processing in EARS-IASI L2

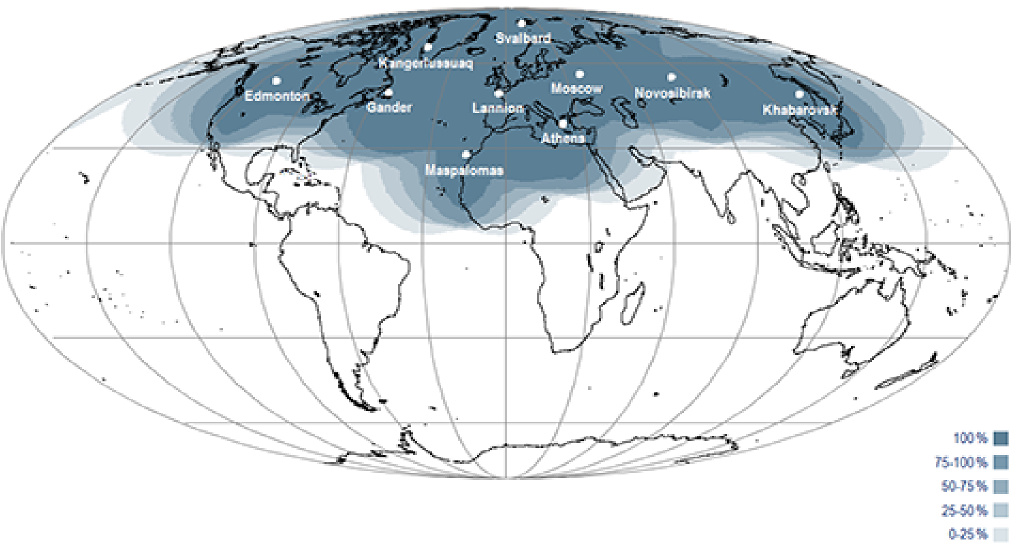

Figure 41: EARS IASI geographical coverage

A summary of direct intercomparisons regional *vs* global all-sky temperature and humidity profiles is presented in the Figure 42 and Figure 43, respectively. Figure 44 shows the distribution of differences in surface temperature. In these figures, the statistics are not stratified against the surface type or any climatological areas. Instead, land, sea, Polar and temperate regions are combined for the purpose of demonstrating the regional *vs* global consistency.

The regional processing of IASI L2 products implements exactly the same software function and configuration of the PWLR[3] as in the global processing. As expected and previously obtained in extensive regional *vs* global verifications [RD-22], the global and regional soundings are statistically in excellent agreement, with dispersions usually of the order of 0.05 K or below (with a peak above 0.1 K at the surface for Metop-B), and between 0.04 to 0.08 g/kg for humidity in the lower troposphere (peaking above 0.1 g/kg at some levels for Metop-A). Noteworthy, the overall statistics (in blue) include a few stronger departures, lying outside the 3σ range. In addition, robust statistics (in red) were computed within the 3σ range, excluding these outliers which represent a fraction of a percent of the samples analysed. In the robust sample, the temperature from regional and global agree well within 0.05 K and the humidity are very well in agreement within 0.08 g/kg and less. The strongest outliers near the surface are mostly found in elevated regions and coastal areas at high latitudes (see Figure 45). The only difference between regional and global processing, besides running on different computing environment, resides in the input products. The calibration of the L1 inputs [IASI L1c radiances, AVHRR geolocation; AMSU and MHS L1B radiances] is intrinsically slightly different in the regional EARS context as compared to the global processing in EPS ground segment and can explain the negligible statistical noise and the rare outliers reported.

This confirms that systematic and random differences between regional and global products are indeed negligible compared to the typical products precision, an order of magnitude smaller than the required products accuracy (e.g. 0.04 K dispersion *vs* 1 K required tropospheric temperature precision). It can be concluded that the validation results demonstrated for global products are applicable to the regional EARS-IASI L2 sounding.

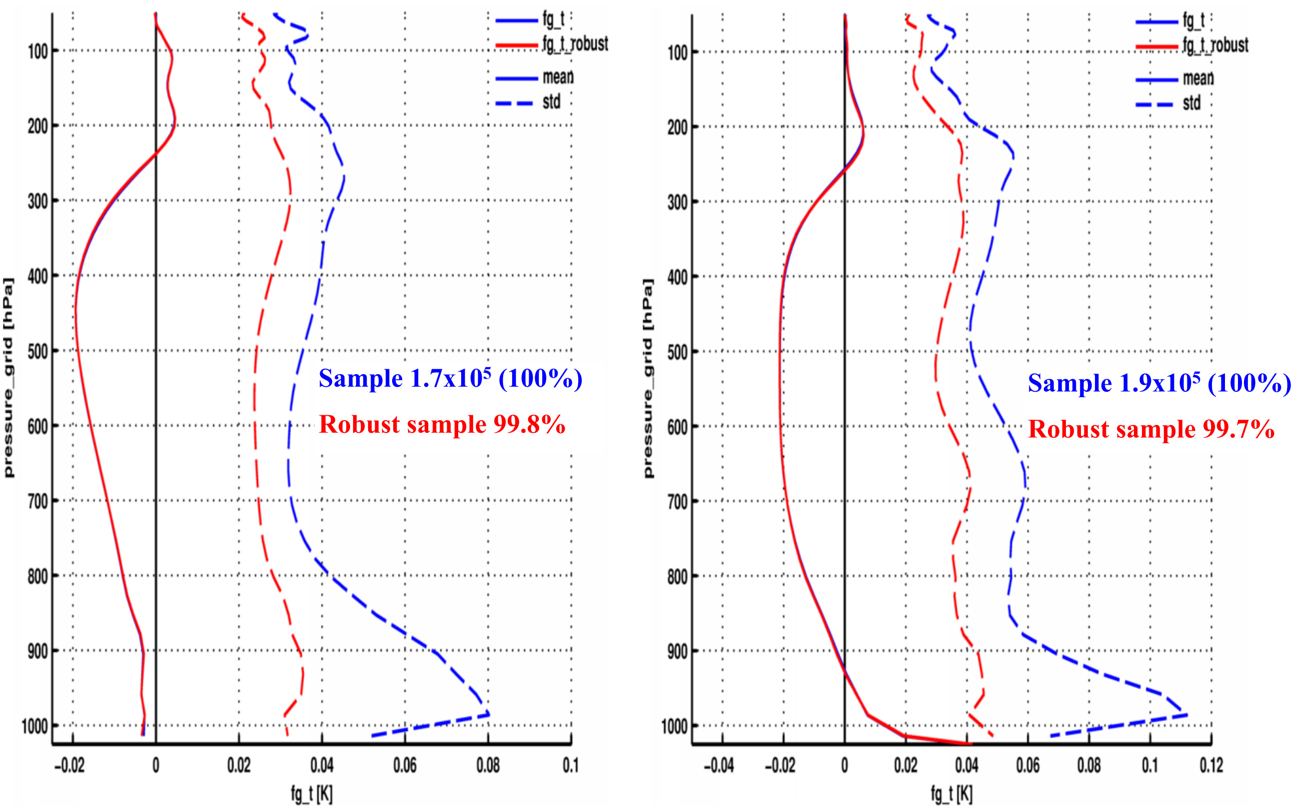

Figure 42: Regional vs global IASI L2 temperature (solid: bias, dash: standard deviation) on 16 February 2018. Overall statistics is in blue and robust statistics (within the ±3σ range) is in red (left: Metop-A, right: Metop-B).

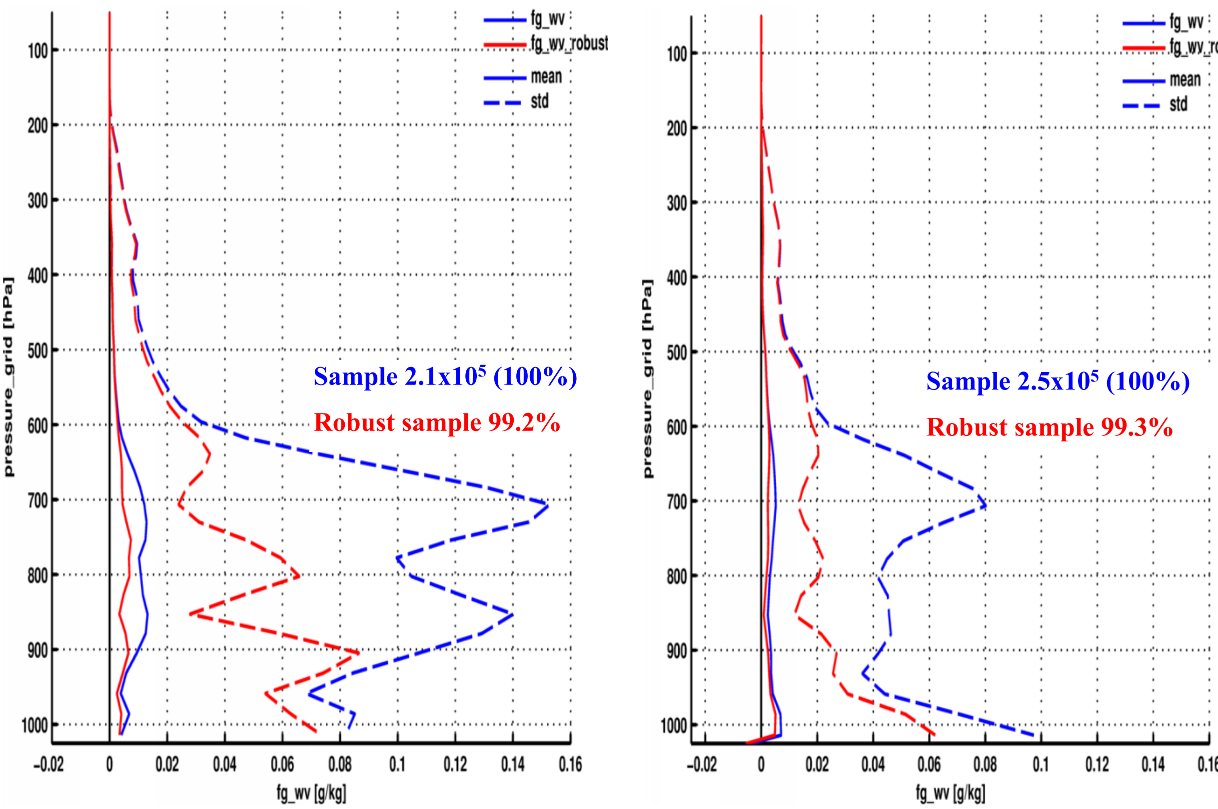

Figure 43: Regional vs global IASI L2 humidity (solid: bias, dash: standard deviation) on 16 February 2018. Overall statistics is in blue and robust statistics (within the ±3σ range) is in red (left: Metop-A, right: Metop-B).

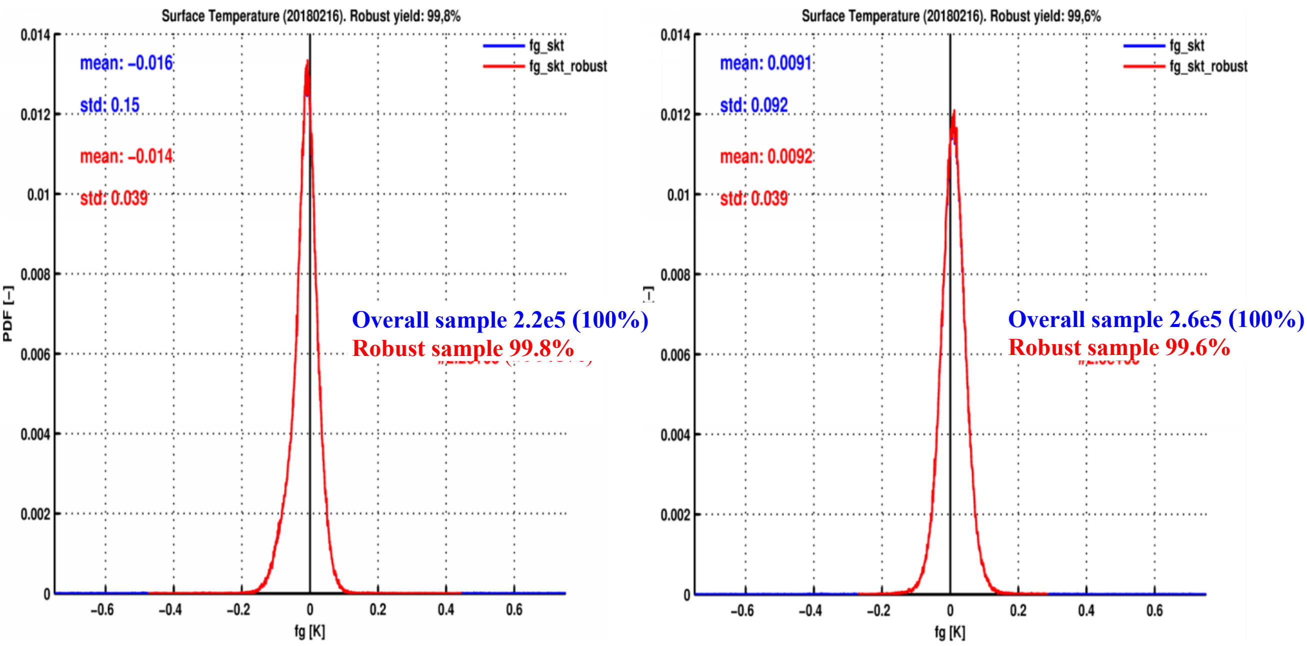

Figure 44: Histogram of the differences between IASI L2 regional and global surface temperature [land and sea combined] on 16 February 2018 (left: Metop-A, right: Metop-B). In blue: overall statistics, in red: robust statistics within 3σ.

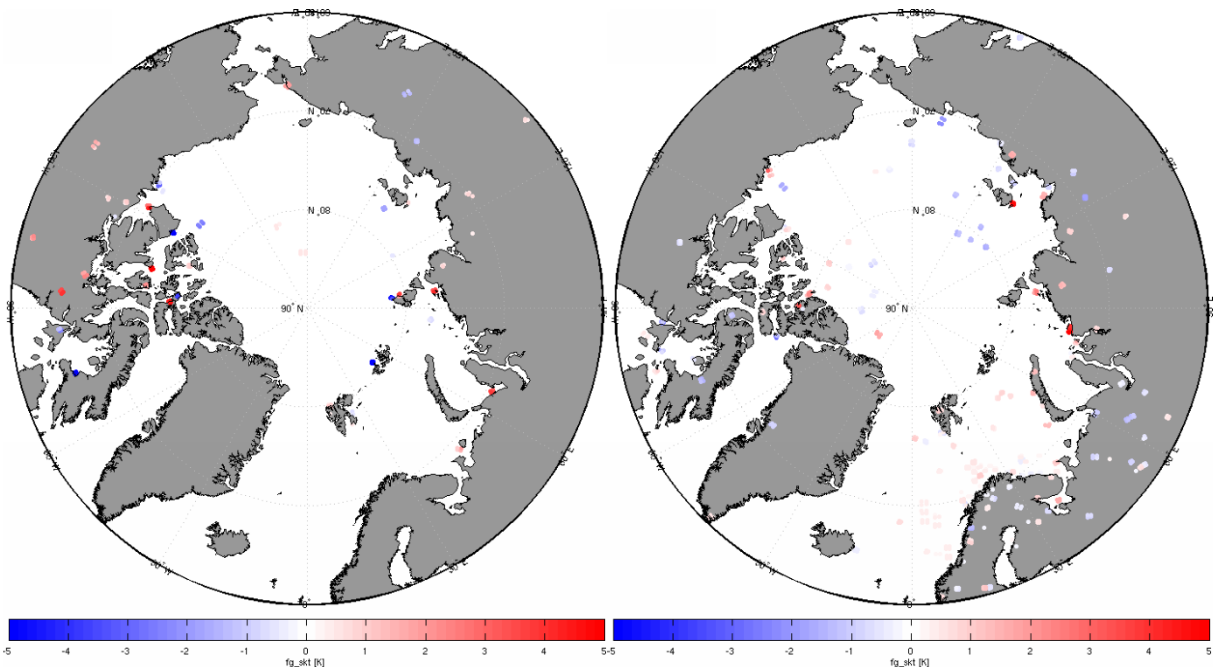

Figure 45: Maps of outliers between regional and global surface skin temperature, for Metop-A (left) and –B (right) on 16 February 2018.

8 SUMMARY AND RECOMMENDATIONS

The main motivations for the revision 6.4 were:

- Correct a small increasing bias in the tropospheric temperature due to the CO_2 static configuration of RTTOV in v6.3 becoming outdated because of the CO_2 rise.
- Improve the infrared-only (IR-only) fall-back mode of the first retrieval with the statistical method PWLR^3 (PieceWise Linear Regression –cube), in the absence of microwave (MW) data.
- Fix an anomaly with rare occurence in the quality control of the SST L2Pcore products

RTTOV in v6.4 has been consequently reconfigured with the latest coefficients, including contemporary CO_2 concentrations. The statistical retrieval (PWLR^3) algorithm was updated with a finer clustering of the regression classes and new training basis, aiming improvements in the IR-only with benefits also in the combined MW+IR modes for atmospheric profiles and for the surface emissivity product. In addition, the v6.4 fixes a few small anomalies in auxiliary processing flags and header information. The classification in quality classes of SST in the L2Pcore has been revised, with an additional check with the quality flag for surface temperature from the PWLR^3.

This report compiles monitoring and validation results performed with *in situ* measurements, numerical model data and inspection of radiance residuals. From this assessment, the following conclusions can be drawn:

i. Temperature and humidity profiles as well as surface parameters are improved compared to v6.3 where expected. No regressions are reported with the introduction of v6.4.
ii. The biases of the first (PWLR^3) and final (OEM) retrievals temperature and humidity profiles have flattened closer to 0 with v6.4 in all locations. The random part of the uncertainty (precision) is also improved in places. OEM retrieved humidity (temperature) in the lower troposphere are for instance 0.1 to 0.2 g/kg (0.1 to 0.2 K) more precise with v6.4 than with 6.3 as assessed with radiosondes and ECMWF analyses. The gain is larger over land, which could also be attributed to better emissivity from the first retrieval, used in the OEM.
iii. The first retrieval (PWLR^3), which is used in the EARS-IASI L2 regional service, is very similar in precision to the OEM; the OEM marginally improving sounding performances, especially over land.
iv. Typical precision in the troposphere in clear-sky with the PWLR^3 and OEM retrievals range between 0.6 and 1 K for temperature and between 0.5 to 1.5 g/kg for humidity for dryer to moister atmospheres. The precision of temperature degrades in the boundary layer, with precision within 1 to 1.5 K over oceans outside the tropics and up to 2 K over land (2.5 K in the surface level).
v. The 'all-sky' products from the first statistical retrieval (PWLR^3) have been analysed against global radiosonde measurements on a 10-month period. Time series of temperature difference show now sign of seasonal signal, e.g. with precision at 500 hPa consistently around 1 K for the 50% best pixels.
vi. The quality indicator for temperature generated with the PWLR^3 was validated through its correlation with the products precision as assessed against sondes, having stratified the retrievals in different quality ranges. It is built as an uncertainty estimate and can be used as a reliable indicator of the expected product precision.
vii. The IR-only retrievals with PWLR^3 are of comparable quality as the MW+IR for their best (clearest pixels) samples. IR-only provides tropospheric temperature sounding with a

precision 1 to 1.5 K including some partly or low-level cloudy pixels (about 30% yield) but the quality degrade to 2 K and above in case of stronger cloud contamination. The MW+IR is more robust to clouds than IR-only, as expected, with larger yield in the best quality classes.

viii. The quality control of SST to form the L2Pcore products with v6.4 yields a more accurate classification in quality levels. The precision in the best 3 quality classes (recommended for use) is improved by 0.05 to 0.2 K in the quality levels 5 (best) to 3 (good). The distribution of the differences between IASI and OSTIA and ECMWF analyses SST is more Gaussian with the v6.4. The new bias characteristics will be assessed with the long-term monitoring against *in situ* buoy measurements. Meanwhile, they have been reset to 0. in the respective SSES (Sensor Specific Error Estimate) auxiliary information.

ix. The land surface emissivity product is slightly improved, which is evident from the radiance fit (OBS-CALC) realised in turn with static emissivity atlases, with v6.4 and v6.3 products.

x. The EARS IASI L2 regional products are consistent with the global 'all-sky' products (retrieved with the PWLR[3]), to within at least an order of magnitude of the absolute required precision [AD-1, AD-2]. Hence, the validation results demonstrated for global products are transferrable to the regional EARS-IASI L2 sounding.

Based on these observations and conclusions, it is recommended to proceed with the operational release of the IASI L2 PPF v6.4, which fixes a few anomalies and enhances the sounding and surface products, and to synchronise EARS-IASI L2 accordingly. The production status of the IASI L2 fields are unchanged.